Natural Hazards
and Earth System
Sciences

Wind-wave characteristics and extremes along the Emilia-Romagna coast

Umesh Pranavam Ayyappan Pillai[1]**, Nadia Pinardi**[1]**, Ivan Federico**[2]**, Salvatore Causio**[2]**, Francesco Trotta**[1]**,
Silvia Unguendoli**[3]**, and Andrea Valentini**[3]

[1]Department of Physics and Astronomy, University of Bologna, Bologna, 40127, Italy
[2]Euro-Mediterranean Center on Climate Change, Lecce, 73100, Italy
[3]Hydro-Meteo-Climate Service of the Agency for Prevention, Environment and Energy of Emilia-Romagna,
Arpae-SIMC, Bologna, 40122, Italy

Correspondence: Umesh Pranavam Ayyappan Pillai (umesh.pranavam@unibo.it)

Abstract. This study examines the wind-wave characteristics along the Emilia-Romagna coasts (northern Adriatic Sea, Italy) with a 10-year wave simulation for the period 2010–2019 performed with the high-resolution unstructured-grid WAVEWATCH III (WW3) coastal wave model. The wave parameters (significant wave height, mean and peak wave period, and wave direction) were validated with the in situ measurements at a coastal station, Cesenatico. In the coastal belt, the annual mean wave heights varied from 0.2–0.4 m, and the seasonal mean was highest for the winter period (> 0.4 m). The Emilia-Romagna coastal belt was characterized by wave and spectra seasonal signals with two dominant frequencies of the order of 10 and 5–6 s for autumn and winter and 7–9 and 4 s for spring and summer. The wavelet power spectra of significant wave height for 10 years show considerable variability, having monthly and seasonal periods. This validated and calibrated data set enabled us to study the probability distributions of the significant wave height along the coasts and define a hazard index based on a fitted Weibull probability distribution function.

1 Introduction

The wind-induced stress on the sea surface gives rise to wind waves that affect human activities on the coasts (Armaroli et al., 2019). The prevailing wind waves of a region determine the defence performance of coastal and offshore structures, and therefore precise information on wind waves is crucial

for coastal operations and defence systems. During extreme events, the wind waves modify the total water-level elevation, leading to a higher risk of overtopping which can damage infrastructures. The Intergovernmental Panel on Climate Change (IPCC, 2007) has also highlighted the need for a long-term evaluation of wind-wave climate trends for coastal resilience (Hemer et al., 2012). The IPCC (2021) indicates the necessity of a regional evaluation of climate change, with various target factors that can aid in risk management and policy-making. The report points out that over the 21st century, nearshore regions will encounter sea level rise, thereby adding to more persistent coastal flooding (across low-lying regions) and associated coastal erosion.

Across the globe, wave climatology studies using re-analysis data sets and model hindcasts have been reported by Carter et al. (1991), Sterl et al. (1998), Young (1999), Cox and Swail (2001), Sterl and Caires (2005), Hemer et al. (2010), Semedo et al. (2011), Young et al. (2011), Zheng et al. (2016), and De Leo et al. (2020). Wind speed and wave height climatologies with emphasis on the Southern Ocean are described in the works of Young (1999), Young and Holland (1996), and Young and Donelan (2018). Past studies on regional scales (Young et al., 2020) based on observations and numerical modelling have also been reported by various researchers on different regions such as the Northern Hemisphere (Woolf et al., 2002; Reistad et al., 2011), the Southern Hemisphere (Gorman et al., 2003), the Mediterranean Sea (Lionello and Sanna, 2005; Lionello, 2012; Clementi et al., 2017; Ravdas et al., 2018; Morales-Márquez et al., 2020;

De Leo et al., 2021; Barbariol et al., 2021; Amarouche et al., 2022), the Persian Gulf (Kamranzad et al., 2013), western Australia (Bosserelle et al., 2012), the eastern North Atlantic (Dodet et al., 2010), the southeast Pacific Ocean (Aguirre et al., 2017), the Indian Ocean (Stopa and Cheung, 2014), the Black Sea (Akpinar and Komurcu, 2013; Arkhipkin et al., 2014; Fedor and Stanislav, 2020), and the China seas (Zheng and Li, 2015; Qian et al., 2020).

Numerous studies have been reported for the Adriatic Sea, using numerical models to demonstrate the wind-wave climate characteristics. In the Adriatic there are many wind-wave forecast systems, including the Henetus forecast system described in Bertotti et al. (2011). Other state-of-the-art models include the Nettuno system as reported in Bertotti et al. (2013), which combines the atmospheric model COSMO (Steppeler et al., 2003) and the wave model WAM (Komen et al., 1994), and SWAN-MEDITARE, which combines COSMO with SWAN (Valentini et al., 2007; Russo et al., 2013). Donatini et al. (2015) have also implemented high-resolution model chains for wind-wave forecasting in the Mediterranean and Adriatic seas, which use a combination of the atmospheric model WRF and wave model MIKE 21 (DHI, 2017). In a study over the Gulf of Taranto in southern Italy, a multi-nesting approach was adopted to evaluate coastal wave dynamics and hydrodynamics (Gaeta et al., 2016). In the Adriatic Sea, Sikiric et al. (2018) implemented the unstructured grid WAVEWATCH III (WW3) (WW3DG, 2016) with 2 km wind forcings from ALADIN forecasts (Farda et al., 2007). The study showed a good match with satellite measurements (SARAL) as compared to CryoSat-2 and Jason-2. The results were in agreement with the studies by Sepulveda et al. (2015), which showed that SARAL estimates of wave heights were far better than CryoSat-2 and Jason-2. Cavaleri et al. (2018) also reported on the application of SARAL data, producing good results.

In a study of the northern Adriatic, Lionello et al. (2012) used the WAM model to predict extreme wind waves and associated storm surge effects. In the Adriatic a modelling combination of WAM + SHYFEM (Komen et al., 1994; Umgiesser et al., 2014) forced with analysis and forecast ECMWF winds was used to forecast the 29 October 2018 storm (Cavaleri et al., 2019) conditions in northern Italy. The application of corrected forecast winds (ECMWF) within these models provided consistent results in line with measurements. High waves in the northern Adriatic Sea were reported in a recent study by Cavaleri et al. (2021).

Studies by Katalinić et al. (2015) reported that in the Adriatic basin, the wind speed and wave height increase from the northern to the southern areas with a maximum mean (annual) H_s of 0.68 m. These results are underestimated as compared with the findings of Queffeulou and Bentamy (2007) resulting from a 14-year (1992–2005) satellite mission that revealed a mean H_s of 0.85 m. Queffeulou and Bentamy (2007) also showed that in the Adriatic Sea, 80 % of the H_s values were lower than 1.10 m. An intercomparison of WAM and WW3 models in the Adriatic and North Sea, based on testing various input physics, was reported by Benetazzo et al. (2021). The analysis aided in investigating the processes that lead to the generation of higher waves in the context of storms.

In the light of several hazardous and extreme events in the Emilia-Romagna (ER) coastal area, several studies have investigated the following: (i) coastal risk and vulnerability to flooding and erosion (Armaroli et al., 2009, 2019; Sekovski et al., 2015; Armaroli and Duo, 2018; Sanuy et al., 2018; Ferrarin et al., 2020); (ii) sea level rise, land subsidence, and littoral hydrodynamics (Perini et al., 2017; Gaeta et al., 2018); (iii) identification of storm thresholds (Armaroli et al., 2012); and (iv) forecasting of coastal flooding (Biolchi et al., 2021, 2022).

To the best of our knowledge, no studies have been carried out to date on the wind and wave characteristics and extremes in the ER coastal belt with high-resolution wind-wave models. Our study focusses on the prevailing wind-wave climatology in the coastal belt of the ER (northern Adriatic Sea) for a period of 10 years (2010–2019), the characterization of the wind-wave regimes, and the study of extreme wave conditions along the coastal belt to quantitatively determine the extreme wave hazard. We use a specific probability distribution function fitting procedure with the wind-wave model data and thereby extract hazard indices for different coastal points. We believe that our 10-year model simulation with appropriate validation at a coastal location will be useful for hazard estimations along the ER coastal area. For the first time we discuss the probability distribution of waves that are essential to quantify the extremes and their hazard.

The paper is organized as follows. Section 2 outlines the study area. Section 3 describes the wind-wave model used in the study, the model forcing, and the validation buoy data used. Section 4 describes the wind and wave climate in the ER coastal belt together with the wave spectra characteristics and wavelet analysis. Section 5 presents the analysis of the probability density distribution and the hazard index for extreme events. Finally, Sect. 6 summarizes the key findings from the study with a brief conclusion.

2   The study area – the Emilia-Romagna coast

The study area is the coastal waters of Emilia-Romagna, situated in northern Italy along the Adriatic Sea, with a coastline including natural zones and dunes to long stretches sheltered by groynes and breakwaters (Armaroli et al., 2012). The coastline is 130 km long (Harley et al., 2016) with the Po Delta as the northern boundary and the town of Riccione at the southernmost point. Figure 1 shows the study area in the ER coastal belt.

There are two main wind patterns in this region – the bora and sirocco winds (Pandzic and Likso, 2005; Umgiesser et al., 2021). Severe wind storms occur from the east-northeast,
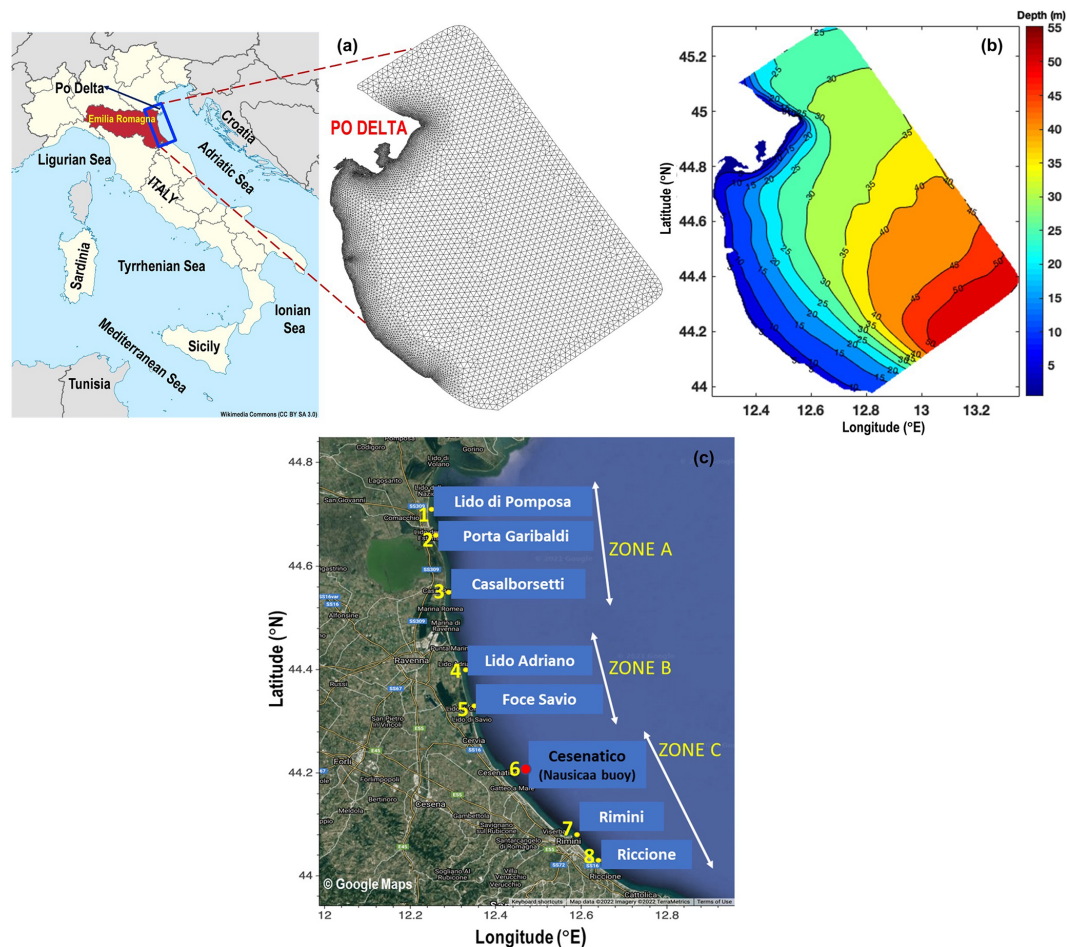
Figure 1. (a) The Emilia-Romagna coastal belt with the unstructured mesh, **(b)** bathymetry for the model domain, and **(c)** the control points across the coastal belt used for analysis and validation. The Nausicaa buoy in Cesenatico (at station 6) was used in this study to validate the hindcast wave parameters.

i.e. the prevailing direction of the bora winds. The sirocco winds are associated with low-pressure systems over the Italian Peninsula and the Ionian Sea. Owing to the restricted fetch, i.e. limited extension of the wave generation area, the bora winds generate young and steep waves that break frequently (Cavaleri et al., 1991), while the sirocco winds generate longer-fetch waves across the Adriatic Sea (Cavaleri, 2000). Thus the swell seas are controlled by the sirocco winds and the seas are dominated by the bora winds (Bonaldo et al., 2017).

The ER coastal area is subdivided into three major zones (Fig. 1c) which correspond to different coastal trophic conditions (Fiori et al., 2016). The station locations are the land town locations perpendicular to which the environmental agency monitoring transects are carried out monthly and weekly to monitor the marine ecosystem environmental status. Thus, knowing the prevailing winds and waves at these locations could be of importance for the management of this important coastal area.

The prevailing hydrodynamics show that the region is microtidal with spring tides (80–90 cm) and neap tides (30–40 cm), with strong diurnal and semi-diurnal components (Armaroli and Duo, 2018). A low-energy wave climate (IDROSER, 1996; Ciavola et al., 2017) has been reported along the coastal belt of ER, i.e. 60 % $H_s < 1$ m. Armaroli et al. (2012) reported that waves originating from the east correspond to a proportion of 91 % $H_s < 1.25$ m, owing to the controlled fetch.

3   Numerical wave model set-up

In this study, the third-generation unstructured-grid spectral-wave model, WW3 (version 5.16; WW3DG, 2016) was used to evaluate nearshore waves. WW3 is a universally accepted wave model (Tolman et al., 2002) with continuous updates of ocean wave physics. The model is formulated by solving the action-density balance equation:

$$\frac{\partial N}{\partial t} + \frac{1}{\cos\phi} \frac{\partial}{\partial\phi} \dot{\phi} N \cos\theta + \frac{\partial}{\partial\lambda} \dot{\lambda} N + \frac{\partial}{\partial k} \dot{k} N$$
$$+ \frac{\partial}{\partial\theta} \dot{\theta}_g N = \frac{S}{\sigma}. \qquad (1)$$

The left-hand side of Eq. (1) denotes the changes in wave action density (i.e. local rate), generation in physical space, shifting of action density (frequency/direction) owing to spatio-temporal changes in depth, and current. λ denotes longitude, φ latitude, θ direction of wave propagation, and k wave number, and σ and t represent the intrinsic angular frequency and time respectively. The source term used in this paper, S in Eq. (1), is the wind input and dissipation source package ST4 (Ardhuin et al., 2010) or ST6 (Zieger et al., 2015; Rogers et al., 2012; Babanin, 2011), the bottom friction JONSWAP (Joint North Sea Wave Project) parameterization (Hasselmann et al., 1973), or SHOWEX (Shoaling Waves Experiment) formulation (Ardhuin et al., 2003) for sandy bottoms. In the section on sensitivity experiments we used a combination of these source terms.

The WW3 model grid (Fig. 1) is divided into 15 392 elements, linked with 8148 nodes, with a resolution of about 300 m at the coast and 2.5 km at the open boundary (Fig. 1a). The merged European Marine Observation and Data Network (EMODnet) data (250 m resolution) and multibeam high-resolution measurements from Arpae (Regional Agency for Prevention, Environment and Energy of Emilia Romagna) serve as the bathymetry of the ER domain (Fig. 1b). The model spectrum is sampled in 24 directions and 30 frequencies (0.0500–0.7932 Hz), with an increment factor of 1.1. The model time steps are set as the (i) maximum global time step, 200 s; (ii) maximum CFL (Courant–Friedrichs–Lewy) time step X–Y, 50 s; (iii) maximum CFL time step k–θ, 50 s; and (iv) minimum source term time step, 10 s. The source term for linear input and wind input uses the parameterization formulated by Cavaleri and Malanotte-Rizzoli (1981) and Donelan et al. (2006). The Generalized Multiple DIA (GMD) was used to simulate the non-linear interactions (Tolman, 2010, 2013, 2014); the dissipation physics were based on Rogers et al. (2012); and the SHOWEX formulations by Ardhuin et al. (2003) were used to simulate the bottom friction. The SHOWEX parameterization is ripple-induced bottom friction, which considers the formation of sand ripples on the bottom. Breaking (depth-induced) is activated using Battjes and Janssen (1978) physics.

The WW3 model is forced every 6 h with the ECMWF analysis winds at 0.125° horizontal resolution. The model winds were validated at three stations, namely Porto Corsini (44.49° N, 12.28° E), Porto Garibaldi (44.67° N, 12.24° E), and Cesenatico Port (44.20° N, 12.40° E) along the ER coastal belt. The wind speed comparison statistics as indicated in Table 1 showed correlations of the order of 0.7, with bias of $-0.2\,\mathrm{m\,s^{-1}}$ indicative of underestima-

Table 1. Quality assessment of ECMWF winds with observed wind speeds for selected stations.

	Wind speed ($\mathrm{m\,s^{-1}}$)				
Statistics	Full year	Winter	Spring	Summer	Autumn
Porto Corsini (year 2013)					
R	0.7	0.7	0.7	0.5	0.7
Bias	−0.2	0.2	−0.1	−0.3	−0.4
RMSE	1.8	1.8	1.9	1.6	2
Porto Garibaldi (year 2018)					
R	0.7	0.8	0.7	0.5	0.8
Bias	−0.2	0.2	−0.3	−0.5	0
RMSE	1.8	1.7	1.6	1.9	1.9
Cesenatico Port (year 2015)					
R	0.7	0.8	0.8	0.5	0.6
Bias	−0.2	0	−0.3	−0.6	0.2
RMSE	1.9	1.7	2	1.9	2

R: correlation; RMSE: root mean square error.

tion of wind speed and RMSE of $1.8\,\mathrm{m\,s^{-1}}$. Larger biases of the order of $-0.6\,\mathrm{m\,s^{-1}}$ and correlations as low as 0.5 exist during summer and some autumn seasons.

The wave lateral boundary values are provided by the Copernicus Marine Environment Monitoring Service (CMEMS) model (https://marine.copernicus.eu/, last access: 20 March 2022; Korres et al., 2021) at a resolution of $\sim$ 4.5 km hourly. The open boundary nodes are forced via JONSWAP wave spectrum approximation (Yamaguchi, 1984) based on the CMEMS wave parameters (significant wave height, peak period, and mean direction).

3.1 Wave observational data set and validation method

In order to validate the model hindcasts, we used the wave buoy Nausicaa in Cesenatico (44.21° N, 12.47° E; station 6) as shown in Fig. 1c. This station is situated away from the coast of Cesenatico municipality and is supported with a Datawell Directional Waverider (MkIII 70 wave) buoy called Nausicaa (https://www.arpae.it/it/temi-ambientali/mare/dati-e-indicatori/dati-boa-ondametrica, last access: 20 March 2022) which has been maintained by Arpae since 23 May 2007. The location of the buoy is 8 km offshore of Cesenatico, at a depth of approximately 10 m, in a region inaccessible to fishing, navigation, and moorings. Wave data such as height (H_s), period, and the direction of waves every 30 min constituted the basic validation data set for the modelling period from January 2010 to December 2019.

Wave model parameters such as wave height, period, and direction were extracted and analysed for eight control points as shown in Fig. 1c. The details of the control points are described in Table 2. The model-simulated 1D wave spectra are extracted and analysed based on seasons.

Table 2. Details of control points 1 to 8.

Control points	Station name	Long (°E)	Lat (°N)	Depth (m)	Zone
1	Lido di Pomposa	12.25	44.71	5.8	
2	Porto Garibaldi	12.26	44.66	5.1	A
3	Casalborsetti	12.29	44.55	5.0	
4	Lido Adriano	12.33	44.40	7.7	B
5	Foce Savio	12.35	44.33	5.3	
6	Cesenatico	12.47	44.21	10.4	
7.	Rimini	12.59	44.08	8.1	C
8.	Riccione	12.64	44.03	6.2	

The skill of the model to reproduce the observations at the Nausicaa buoy location was assessed by standard statistics, namely the correlation coefficient (R), bias, and root mean square error (RMSE):

$$R = \frac{\sum_{i=1}^{n}\left(P_i - \overline{P}\right)\left(O_i - \overline{O}\right)}{\sqrt{\sum_{i=1}^{n}\left(P_i - \overline{P}\right)^2\left(O_i - \overline{O}\right)^2}}, \tag{2}$$

$$\text{bias} = \frac{1}{n}\sum_{i=1}^{n}\left(P_i - O_i\right), \tag{3}$$

$$\text{RMSE} = \sqrt{\frac{1}{n}\sum_{i=1}^{n}(P_i - O_i)^2}, \tag{4}$$

where model estimates are denoted by P, O represents observational data, n indicates number of data points, and the overbar denotes mean values.

3.2 Sensitivity experiments for wave model parameterizations

Three sets of sensitivity experiments using WW3 were executed using a combinations of wave physics:

i. ST4 + JONSWAP (EXP1),

ii. ST4 + SHOWEX (EXP2), and

iii. ST6 + SHOWEX (EXP3),

for the representative months of February (winter) and September (autumn) 2018. The combination of ST6 with JONSWAP is not considered because this bottom friction is not suitable for sandy beaches as EXP1 will show.

The H_s comparison with the Nausicaa buoy is shown in Table 3, which highlights that the best physics is given by EXP3. The mean buoy H_s is 0.92 and 0.38 m for February and September 2018 respectively. The comparison of the mean wave period, T_m (not shown), for the three experiments showed a higher performance using the combination

Table 3. Skill scores for the sensitivity experiments.

Experiment	Significant wave height (H_s in m)					
	February 2018			September 2018		
	R	Bias (m)	RMSE (m)	R	Bias (m)	RMSE (m)
EXP1	0.93	−0.12	0.29	0.92	−0.15	0.21
EXP2	0.91	−0.09	0.32	0.90	−0.12	0.18
EXP3	0.94	−0.04	0.26	0.96	−0.09	0.14

R: correlation; RMSE: root mean square error.

of ST6 + SHOWEX. The sensitivity study produced sufficient confidence in using the ST6+SHOWEX physics for the ER region. This wave physics was thus adopted for the 10-year simulation.

3.3 Validation of wave hindcasts

The model outputs, such as significant wave height (H_s), mean wave period (T_m), peak wave period (T_p), and mean wave direction (θ_m), were compared with the buoy observations for the 10-year period 2010–2019. Figure 2 shows the 10-year comparison of H_s, which qualitatively demonstrates that the overall model H_s also followed the buoy values in peak events at the Cesenatico station (station 6 in Fig. 1c). This is a consistency check of model against observations as required for "goodness" indicators in numerical weather predictions (Murphy, 1993). The model also captures the seasonal variations at the coastal location. In general, the lower H_s values are slightly overestimated, while higher H_s values are underestimated.

Table 4 shows the validation statistics for each year. The mean of model/buoy estimates for H_s, T_m, and T_p are 0.40/0.45 m, 3.02/3.23 s, and 4.17/4.36 s respectively. On average the model underestimates the measurements (as seen from the negative bias for most of the years). A high correlation is shown, ranging from 0.81 to 0.93 for 2010–2019, with the highest correlation for 2017. The T_m comparison revealed a lower correlation of the order of 0.72 to 0.81, compared to H_s. The negative bias (−0.371 to −0.018 s) indicated an underestimation of T_m, with a corresponding RMSE of the order of 0.79 to 0.91 s. Similarly, the T_p also showed a lower correlation (0.53 to 0.70) in comparison to H_s and T_m. T_p also showed underestimations as revealed from the bias of the order of −0.382 to 0.151 s, with an RMSE varying from 1.48 to 1.78 s.

Figure 3 represents the observations–model scatter plot of H_s for the period 2010–2019 (Fig. 3a) and the seasonal scatter as shown in Fig. 3b–e for station 6. The dashed red line denotes the best data fit for the comparison. The comparison of H_s for 2010–2019 (Fig. 3a) shows that there is relatively good agreement between model H_s and measurements with a high correlation of 0.90. There is a slight underestimation (bias = −0.05 m), with RMSE = 0.21 m. The seasonal
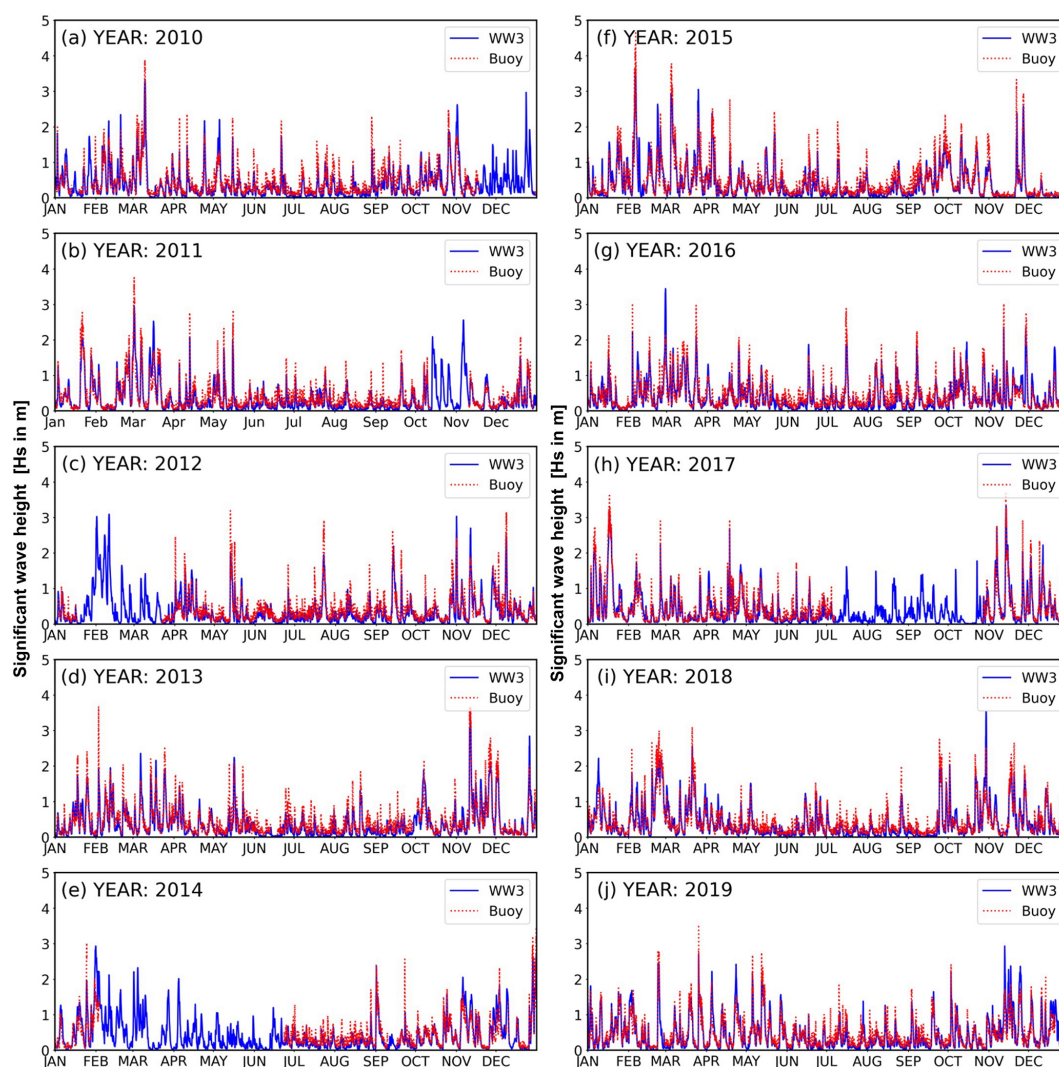
Figure 2. Time series plot of **(a–j)** significant wave height (in metres, indicated by solid blue lines) and observations (dotted red lines) for 2010–2019 at station 6 (Cesenatico; see Fig. 1c for location).

scatters for winter, spring, and autumn (Figs. 3b, c, and e) showed high correlations, with a slight underestimation in relation to buoy observations. The summer seasons (Fig. 3d) showed a comparatively lower correlation with an underestimation of H_s. In general, the model H_s underestimates the buoy data, specifically the higher H_s, and similar underestimations have been reported in many past studies such as Ardhuin et al. (2007), Korres et al. (2011), and Clementi et al. (2017).

The comparison of T_m for 2010–2019 is shown in Fig. 3f and for the seasons in Fig. 3g–j, revealing a larger scatter in comparison to H_s. During 2010–2019 (Fig. 3f), the simulated T_m is lower than the buoy measurements and shows a lower performance ($R = 0.75$) in comparison to H_s. The winter, spring, and autumn seasons (Fig. 3g, h, and j) showed a moderate correlation of 0.74 to 0.75, while the lowest correlation was observed in summer (0.62). For all the seasons,

underestimations of T_m were noted, with the maximum in summer ($B = -0.47$ s) and lowest in winter ($B = -0.11$ s).

## 4   Characterization of the Emilia-Romagna wind and wave fields

4.1   Wind climatology of the Emilia-Romagna coast

Below we present the wind climatology in the ER region based on the ECMWF analysis winds over a period of 10 years. The seasons are presented as winter (December–January–February), spring (March–April–May), summer (June–July–August), and autumn (September–October–November).

Table 4. Statistics of the comparison of buoy measurements (Cesenatico, station 6) with model results for 2010–2019.

Statistics	2010	2011	2012	2013	2014	2015	2016	2017	2018	2019
Significant wave height (H_s in m)										
R	0.882	0.903	0.876	0.814	0.860	0.917	0.890	0.932	0.915	0.897
Bias	−0.055	−0.066	−0.076	−0.065	−0.022	−0.053	−0.045	−0.031	−0.035	−0.016
RMSE	0.211	0.193	0.205	0.211	0.252	0.209	0.201	0.194	0.193	0.206
Mean wave period (T_m in s)										
R	0.718	0.776	0.724	0.739	0.809	0.746	0.740	0.709	0.746	0.777
Bias	−0.23	−0.371	−0.321	−0.255	−0.112	−0.363	−0.194	−0.018	−0.159	−0.071
RMSE	0.911	0.797	0.841	0.872	0.828	0.904	0.804	0.838	0.854	0.821
Peak wave period (T_p in s)										
R	0.653	0.530	0.598	0.621	0.705	0.543	0.603	0.605	0.653	0.642
Bias	−0.305	−0.255	−0.325	−0.273	−0.258	−0.382	−0.183	0.151	−0.084	0.079
RMSE	1.618	1.782	1.611	1.687	1.483	1.860	1.575	1.636	1.597	1.582

R: correlation; RMSE: root mean square error.
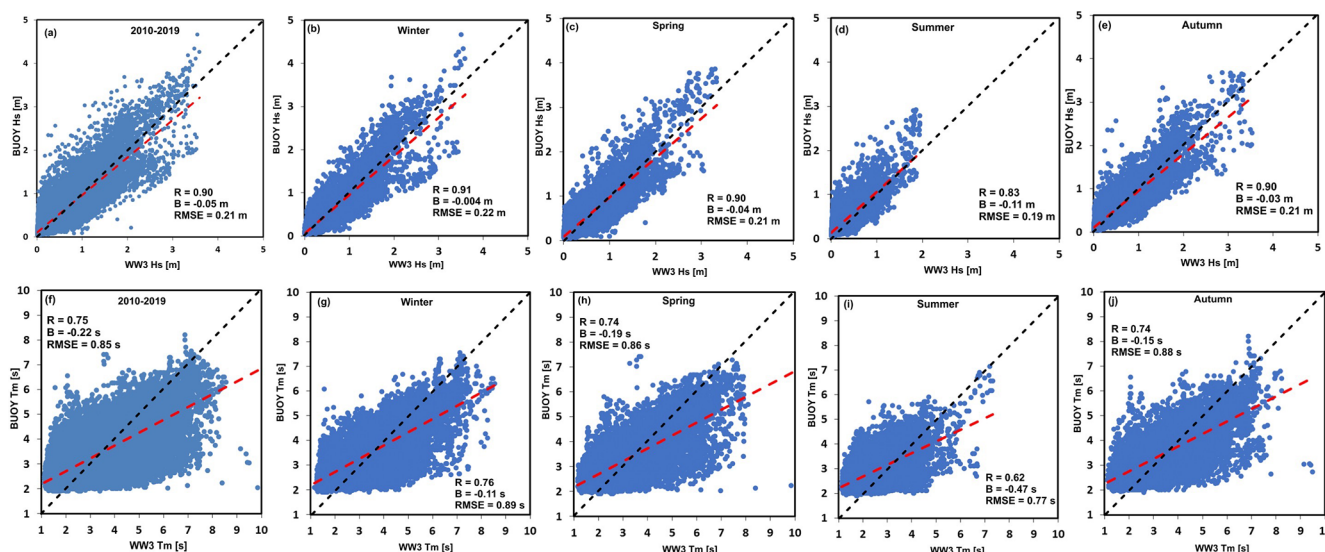
Figure 3. Observations–model scatter plot of H_s (in metres) for **(a)** 2010–2019, **(b)** winter, **(c)** spring, **(d)** summer, and **(e)** autumn (top panels) at station 6 (Cesenatico; see Fig. 1c for location). The bottom panels show scatter plots of the mean wave period (T_m in seconds) for **(f)** 2010–2019, **(g)** winter, **(h)** spring, **(i)** summer, and **(j)** autumn. The dashed black line indicates the best fit (1 : 1 slope), and the dashed red line represents the data fit. (R: correlation; B: bias; RMSE: root mean square error.)

4.1.1 Climatology of wind speed and direction

Analysis of wind speed and direction over the ER coast for the period 2010–2019 is presented in Fig. 4. The annual mean characteristics showed a very precise pattern, with the winds reaching the coast from the east-northeast. The annual mean wind speeds were of the order of 0.5–2 m s^{-1}, with a large standard deviation (SD) of 1.6–3 m s^{-1}.

The lowest wind speeds were observed during spring and summer (1.5 and 1.8 m s^{-1}), followed by autumn (2.4 m s^{-1}), with the highest wind speeds (2.9 m s^{-1}) during

winter. Overall, for the winter and spring the approaching wind is easterly, related to the bora wind climatological direction. In the summer, the mean wind direction is from the southeast, owing to sirocco events. The spatial distribution of the seasonal and annual SD of wind speed from 2010–2019 is shown in Fig. 4f–j. The annual SD varies from 1.6 to 3 m s^{-1} in the entire domain (Fig. 4j), and the annual maximum is further offshore from the ER coastal belt. During the winter (Fig. 4f), the SD varies from 2.2 to 3 m s^{-1} and, in spring, from 1.2–3 m s^{-1} (Fig. 4g). While in summer and autumn, the SDs are 2.2–2.6 and 1.6–3 m s^{-1} respectively.
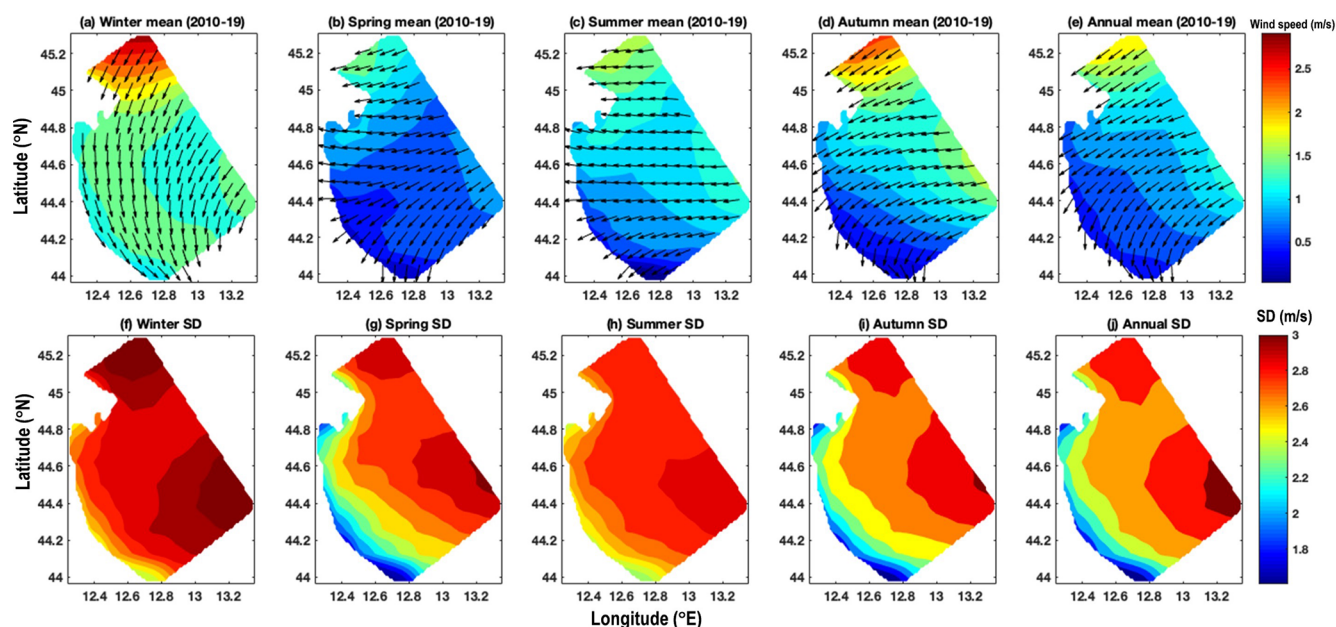
Figure 4. Wind climatology for the Emilia-Romagna region based on ECMWF analysis wind data for 2010 to 2019. Mean wind speed and direction for **(a)** winter, **(b)** spring, **(c)** summer, **(d)** autumn, and **(e)** annual periods (top panels). The lower panels show the standard deviation (SD) of wind speed for **(f)** winter, **(g)** spring, **(h)** summer, **(i)** autumn, and **(j)** annual periods.

To better study the wind characteristics along the ER coast, the wind rose diagrams are shown for the eight control points in Fig. 5a to h. Points 1 to 5, belonging to Zone A and Zone B, have the highest wind speeds, approaching at an angle of 45 to 135°. The wind speed ranging from 3 to $4\,\mathrm{m\,s^{-1}}$ is more frequent at these control points at an approaching angle ranging from 45 to 90°. The average coastal angles of Zone A and Zone B are nearly 45°. Points 6 to 8 fall along the concave side of the coastal area, i.e. in Zone C. Along these control points, the maximum wind speed approaches from W to NNW. The wind speeds up to $3.5\,\mathrm{m\,s^{-1}}$ show a marked increase in frequency. The frequent wind speeds approach from NW and ENE for station 6, NNE for point 7, and NNW for point 8. Moving from point 1 to 8, there is a gentle shift in the maximum wind speed approaching from NNE to ENE.

4.2 Wave climatology of the Emilia-Romagna coast

4.2.1 Wave height and direction climatology

Figure 6 (top panels) depicts the annual mean H_s for the ER coast and the seasonal H_s means for winter, spring, summer, and autumn. The SD for each event is illustrated in the bottom panels from 2010 to 2019. The waves converge at the southern and the northern part of the study domain due to the shape of the coastline. There is divergence in wave energy in the middle region of the coastal domain (i.e. Zone B as reported in Fig. 1c). The annual H_s mean (Fig. 6e) in the domain varied from 0.08–0.6 m. The annual average H_s is

higher (0.5–0.7 m) off the ER coast and at the boundary in the open ocean, and in the central ER domain H_s is of the order of 0.5–0.6 m. However, in the ER coastal belt, the annual mean H_s is < 0.4 m owing to the bathymetric features.

The seasonal climatology of H_s in the winter season (Fig. 6a) indicates higher waves offshore of the order of 0.1–0.9 m, where the ER coastal belt has H_s < 0.5 m. In spring (Fig. 6b) and summer (Fig. 6c) the H_s values are comparatively lower and vary in the range of 0.1–0.5 and 0.1–0.33 m respectively. The autumn H_s mean in the ER coastal belt is < 0.4 m. The spatial H_s field structure and direction approximately resemble the bathymetric contour lines (Fig. 1b). The annual SD (Fig. 6j) varies from 0.09–0.71 m in the ER domain. The summer season (Fig. 6h) shows the lowest SD (0.1–0.38 m) compared to all other seasons.

The detailed features of the model in the coastal zone are shown by means of wave rose diagrams (Fig. 7) for the eight points in Fig. 1c. The waves at control point 1 fall in the Lido di Pomposa region where the coast is sheltered and exposed to winds and marine currents. The bathymetric contour enables the waves to converge in control point 1, where the maximum wave heights approach from E to SE. From points 2 to 7 along Porto Garibaldi to Rimini, the approaching angles of wave heights are from NE to SE. The maximum waves approach from ENE to E for points 2 to 4 and NE to E for points 5 to 8. The maximum wave activity is observed at point 3. Point 1 is a relatively calm area compared to the other control points, perhaps because of the shadow zone. The concave shape of the coast, well represented by the high-resolution unstructured-grid model, and bathymetric patterns
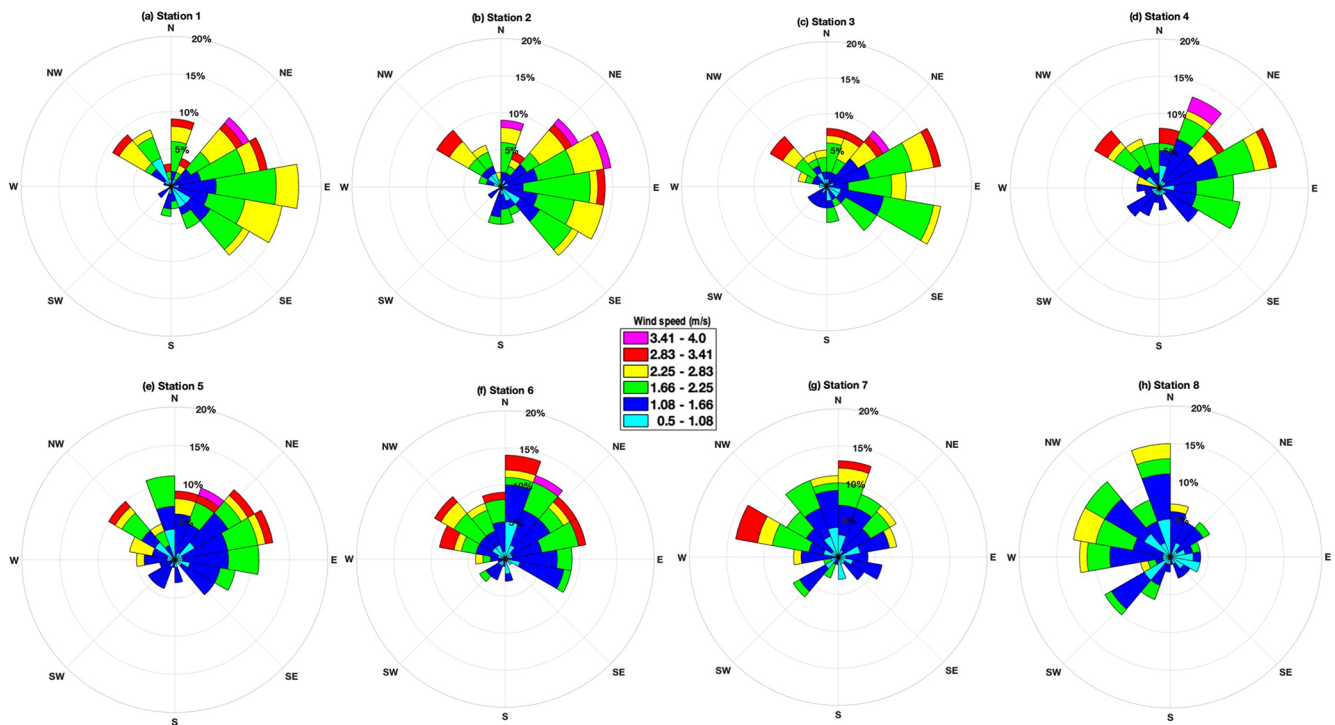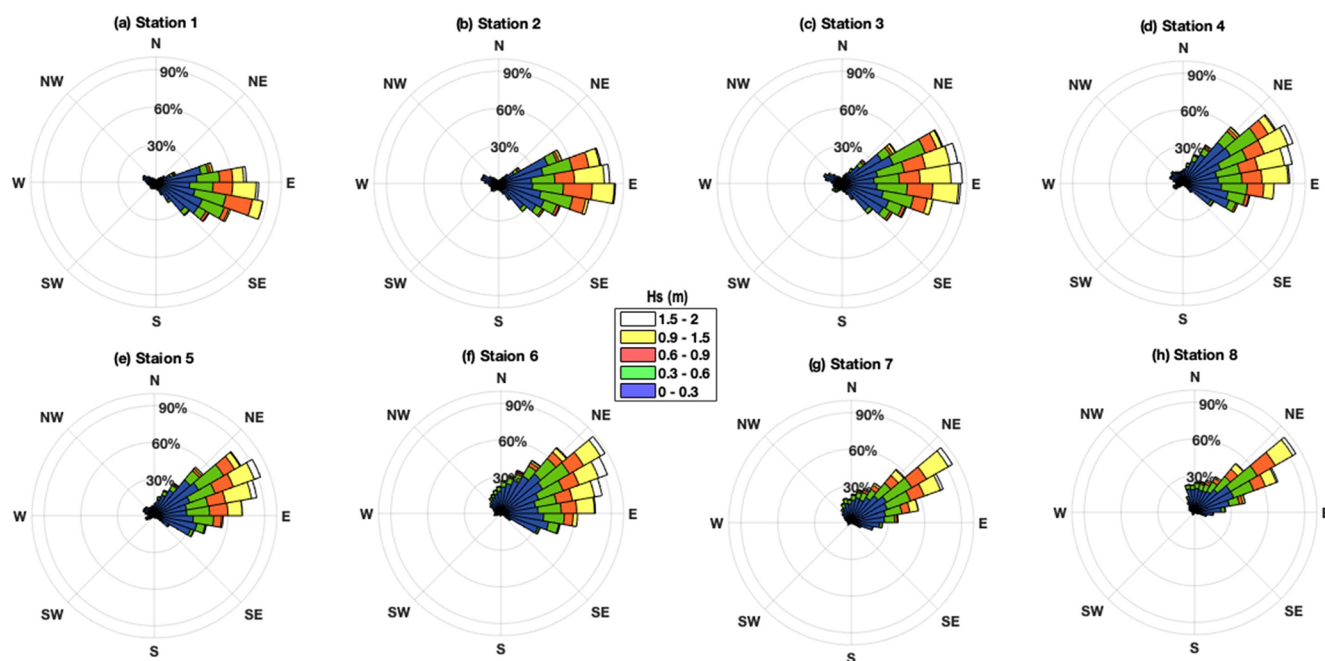
Figure 5. Wind rose diagrams at the control points shown in Fig. 1 based on monthly average winds throughout 2010–2019. The wind rose shows the direction the winds come from (N: north; NE: northeast; E: east; SE: southeast; S: south; SW: southwest; W: west; NW: northwest).
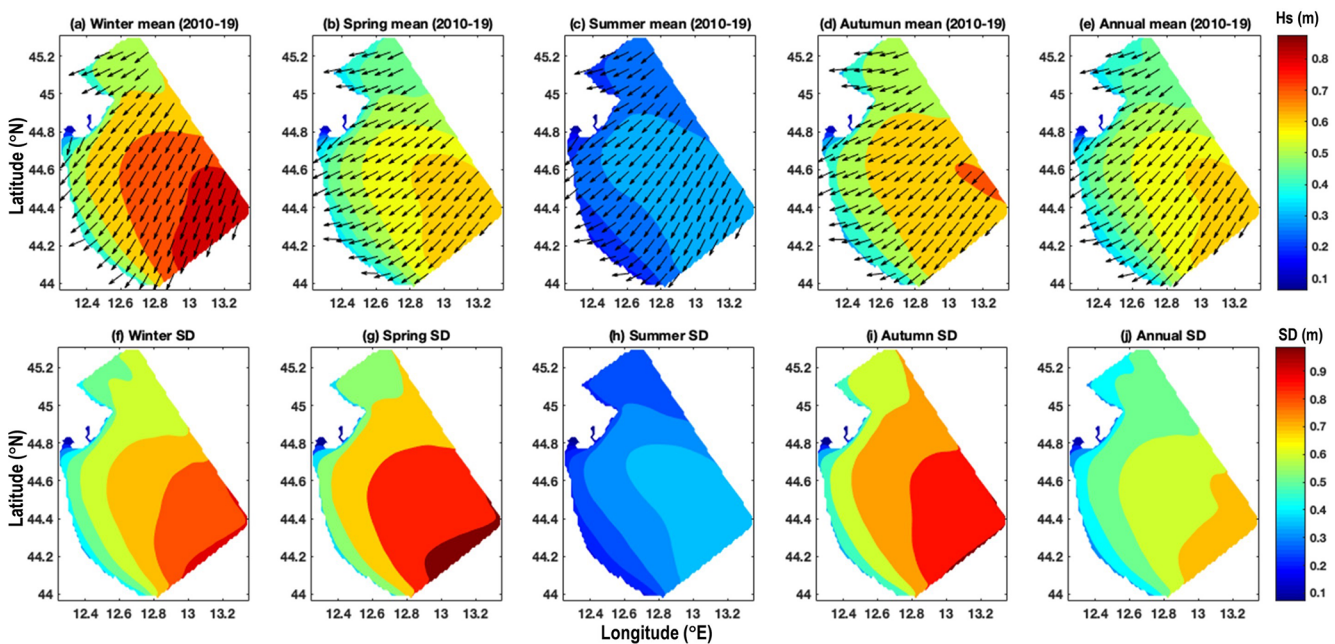
Figure 6. Wave climatology for the Emilia-Romagna region for 2010 to 2019. Mean significant wave height and direction for **(a)** winter, **(b)** spring, **(c)** summer, **(d)** autumn, and **(e)** annual (top panels). The lower panels show the standard deviation (SD) of wave height for **(f)** winter, **(g)** spring, **(h)** summer, **(i)** autumn, and **(j)** annual periods.

Figure 7. Nearshore wave climate: wave rose diagrams in the coastal belt of Emilia-Romagna along control points 1 to 8 (see Fig. 1c). The wave rose indicates the direction the waves come from (N: north; NE: northeast; E: east; SE: southeast; S: south; SW: southwest; W: west; NW: northwest).

are key to understanding the prevailing wave characteristics in the ER coastal belt. The wave energy converges at the end points and diverges at the middle points.

Based on available buoy data for the Cesenatico station, the observed wave roses are compared with the model estimates for selected years as shown in Fig. 8. Overall, the modelled wave roses (Fig. 8b, d, and f) show reasonable correspondence with the observed data (Fig. 8a, c, and e), even with some difference in magnitudes. An underestimation of model wave heights in the lower ranges is noted. Comparing the directional distribution of waves, the directions are comparable and in the same sectors but there exist higher differences in their magnitudes. A similar wave climate by the Nausicaa buoy located offshore of Cesenatico is reported in studies by Armaroli et al. (2012) and Romagnoli et al. (2021), which shows that this is the representative wave climate of the Emilia-Romagna coast. This qualitative comparison shows that at the Cesenatico station, overall characteristics of waves are fairly reproduced by the model.

Figure 9 shows the offshore wave climate, presented as wave rose diagrams at the control points along the boundaries of the study domains (control points 9 to 14). In Fig. 9a at point 9, the waves approach from NE to SE with maximum H_s approaching from ENE to ESE. At point 10, the predominant waves are at an angle of 30 to 150° where the maximum H_s approaches from NE and SE directions (see Fig. 9b). For points 11 to 14, the predominant wave directions are from 30 to 150°, where the maximum H_s approaches from NE and

SE directions. Deep-water control points 10 to 14 receive waves from all directions.

4.2.2 Wave spectra characteristics

In the ER region, there are hardly any studies on the spectral characteristics of the waves. Cavaleri et al. (2019) analysed model spectra for the event of 29 October 2018 in the northern Adriatic Sea and compared them with measurements on the Venice coastline. The simulated wave spectra on the 25th of the months corresponding to winter (February), spring (May), summer (August), and autumn (November) at 12:00 LT are represented in Fig. 10a to d for station 6 for 2010–2019.

Figure 10a shows the simulated instantaneous spectra in February (25th of the month, 12:00 LT) with the highest peak energy of $2.0234\,\mathrm{m^2\,Hz^{-1}}$ for 2018 and the lowest of $0.0008\,\mathrm{m^2\,Hz^{-1}}$ for 2012 and 2014. February, which is a representative month of the winter season, shows a combination of single-peaked and double-peaked spectra with swell dominance at the coastal location. In all the seasons, the swell dominates the spectral energy with a peak at around 0.11 Hz (9 s). The shorter wave peaks range from 0.21 to 0.54 Hz (1.8 to 4.7 s). The spectra vary considerably over the years, and in general, the wave spectra at the Cesenatico coastal location showed signatures of single- and double-peaked spectra for the period 2010–2019 (Table 5). The wave spectra were prominently double-peaked during all seasons (45 %–53 %), along with single-peaked spectra but with a lower percent-
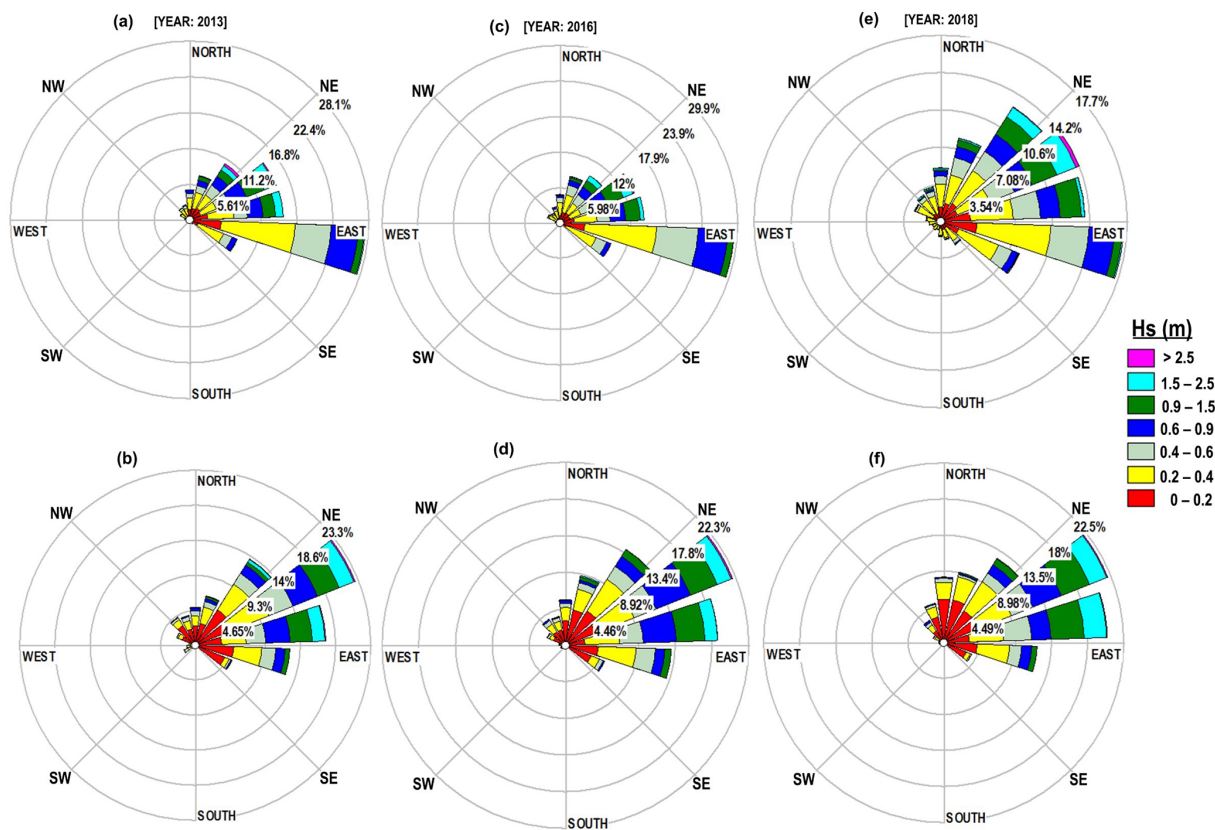
Figure 8. Comparison of directional histograms of wave heights: buoy (**a, c, e**), and simulated (**b, d, f**) data at Cesenatico, station 6 (NE: northeast; SE: southeast; SW: southwest; NW: northwest).

Table 5. Number of occurrences of single-peaked, double-peaked, and multi-peaked spectra at Cesenatico location for different seasons (2010–2019).

Seasons (2010–2019)	Single peak (%)	Double peak (%)	Multi-peak (%)
Winter	31	45	24
Spring	32	45	23
Summer	27	53	20
Autumn	33	49	18

age of occurrences (27 %–33 %). Double peakedness was highly prominent in the summer season (53 %), while winter, spring, and autumn showed dominance of single-peaked spectra (31 %–33 %). As evident from Table 5, the percentages of the number of peaks (single/double) in the Cesenatico location clearly depict the co-existence of sea-swell characteristics in the study domain.

The monthly mean wave spectra for winter, spring, summer, and autumn corresponding to the typical months of February, May, August, and November for 2010–2019 are represented in Fig. 11a to d. During February (Fig. 11a), the averaged spectra showed prominent single peaks for most

of the years with peak energies of the order of 0.1615–0.722 m^2 Hz^{-1}. The highest peak energies were in 2012 (0.701 m^2 Hz^{-1}) and 2014 (0.722 m^2 Hz^{-1}), and during the 10-year period the peak frequencies ranged from 0.0974 to 0.1726 Hz. Figure 11b shows the averaged spectral characteristics for May (spring). As seen from Fig. 11b, 2019 had the highest peak energies of 0.253 m^2 Hz^{-1}, and the spectra also highlight a few secondary peaks in some of the years with the peak frequency ranging from 0.1072 to 0.2297 Hz. During the summer season (August), the spectra show single/double peaks with peak energies varying from 0.0102 to 0.0686 m^2 Hz^{-1} (Fig. 11c). The maximum peak energy was for 2016 (0.0686 m^2 Hz^{-1}) with comparatively low energies for the rest of the years and with peak frequencies varying from 0.1427 to 0.278 Hz. Similarly, during autumn (Fig. 11d), the averaged spectra were mostly single-peaked with peak energies of the order of 0.1362 to 0.740 m^2 Hz^{-1}. The highest peaks with energies of 0.740 m^2 Hz^{-1} were in 2019, with the lowest energy in 2015. The dominant frequencies corresponding to the peak energies were 0.0974–0.2089 Hz.

Overall, the highest and lowest spectral peaks are in winter and summer, with energies of 0.722 and 0.0686 m^2 Hz^{-1}, as shown in Fig. 11a and c. The mean wave spectra for 2010
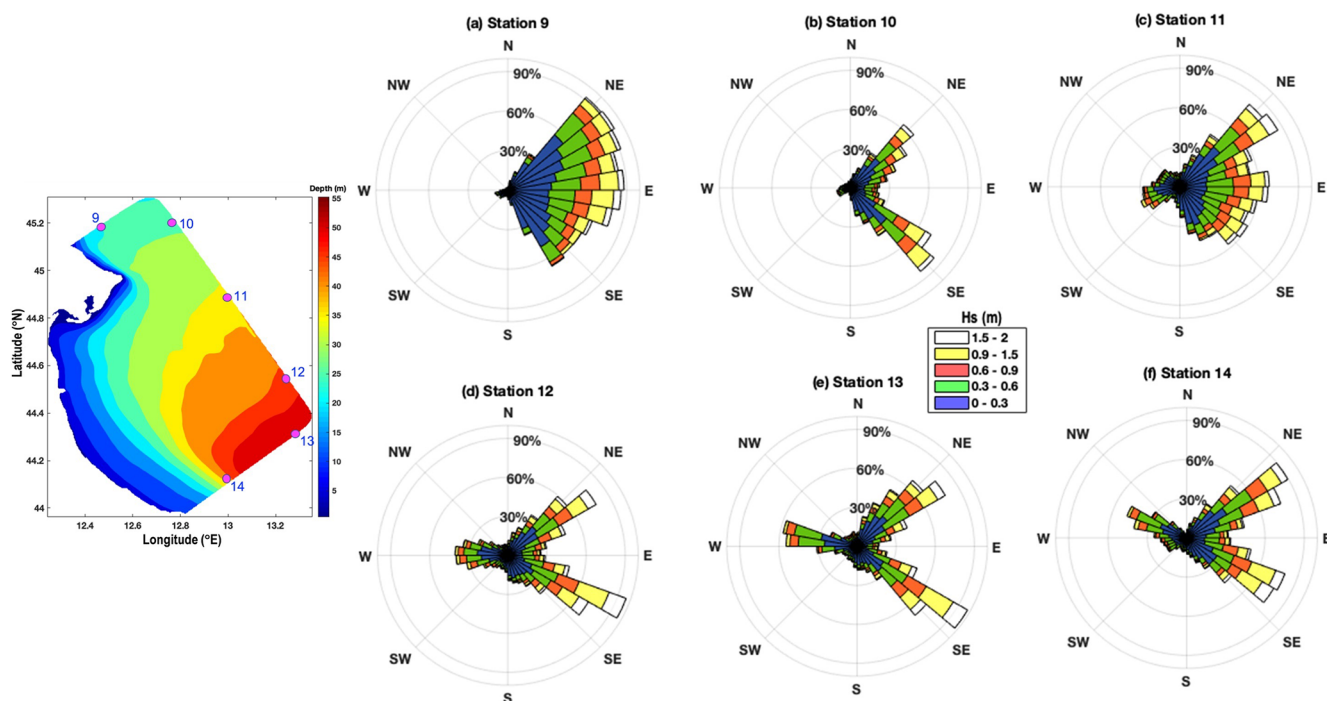
Figure 9. Offshore wave climate: wave rose diagrams in the boundaries of the model domain for the control points (9 to 14) as indicated in the location bathymetric map shown adjacently (left) (N: north; NE: northeast; E: east; SE: southeast; S: south; SW: southwest; W: west; NW: northwest).

to 2019 exhibit a peak in variance for 2014, 2019, 2016, and 2019 for winter, spring, summer, and autumn respectively. The spectra show more or less similar characteristics for spring and autumn. There is also a reversal of spectrum curves for winter and spring as swells clearly dominate the coastal location. The spreading of spectra, which is dependent upon the wind characteristics and the prevailing fetch, is variable during all seasons.

4.2.3 Wavelet analysis

Wavelet analysis is an important tool to analyse spectral components and occurrence time (Torrence and Compo, 1998). The wavelet considers spectral components' time localization, as well as time–frequency rendering of signal into realization, such that the frequencies in the wavelet analysis are associated with the time domain. Thus, wavelet analysis (based on the Morlet mother wavelet) provides an understanding of spectral characteristics and their variability in time.

In this study the wavelet transform for H_s (Fig. 12) was applied to the coastal location of Cesenatico for 2010–2019, using the mean model estimates. Figure 12a represents the wavelet power, with the x axis representing the time and y axis denoting the component periods. Figure 12b represents the global wavelet power spectrum, i.e. time-averaged power spectrum, which uses the same y axis. Cesenatico was selected as it was the station where the wave parameters were

validated with the model estimates. The idea of presenting the wavelet transform is to accurately represent the variance in the spectrum. In the power wavelet (Fig. 12a), the real signals can be observed enclosed in the black contours with a 95 % confidence level, while the region below the dashed magenta line indicates the cone of influence, in which the time series analysis edge effects are significant. In the global spectrum, the peaks indicate the combined signal throughout the analysis. The dashed red line in the global spectrum corresponds to a confidence level of 95 %.

In Fig. 12, the largest signal occurs in the 256–512 d band, which contains the seasonal frequency, and sporadic signals can be identified by comparatively short times (2–3 months). Figure 12a indicates that over the 10-year period, intermittent oscillations are in band 16–128 in the years 2011, 2012, 2014, 2016, 2018, and 2019. Figure 12c shows the 16–512 d period of the scale average H_s time series, with 95 % significance denoted by a dashed red line. Significant peaks can be seen in 2014, 2015, 2016, and 2019, while 2019 shows the highest variance. From 2010 to 2013 and 2017 to 2018, the peaks showed lower amplitudes. The seasonal signal is very different from year to year with peaks occurring sometimes only during the autumn.
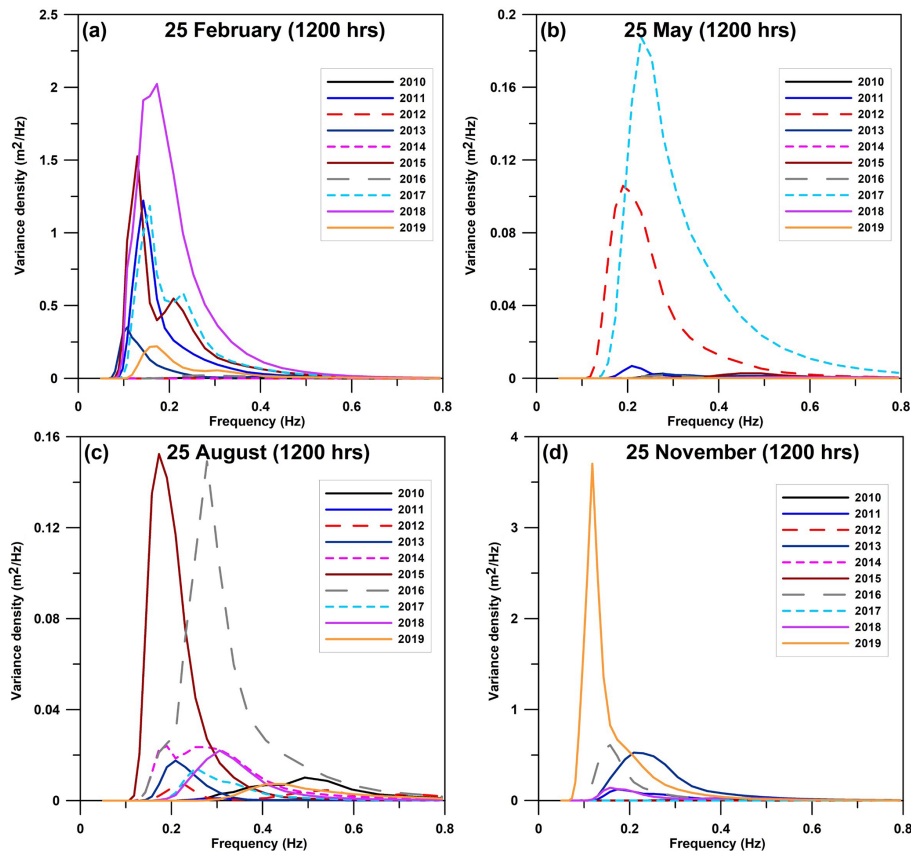
Figure 10. Simulated wave spectra for 2010–2019 on the 25th day (12:00 LT) of **(a)** February (winter), **(b)** May (spring), **(c)** August (summer), and **(d)** November (autumn) at station 6 (Cesenatico; see Fig. 1c for location).

5 Extreme-wave analysis

In this study, the statistical characteristics of H_s were analysed using the methodology of fitting a probability distribution function (PDF) to the wave time series at the control points of the ER coastal belt. Many studies have indicated that the probability distribution used to model long-term distributions of wave heights is well represented by the two-parameter Weibull distribution (Muraleedharan et al., 1993, 1998, 1999). The PDF of a random variable x with the Weibull distribution (Weibull, 1951) is defined for positive values, $x > 0$, as

$$f_W(x; \lambda, \kappa) = \frac{\kappa}{\lambda} \left(\frac{x}{\lambda}\right)^{k-1} \exp\left[-\left(\frac{x}{\lambda}\right)^k\right], \qquad (5)$$

where κ and λ (> 0) are the shape parameter (dimensionless) and scale parameter (m) respectively. It is clear that when $\kappa = 1$, the PDF reduces to an exponential distribution. Fitting this PDF to the data enables the hazard index to be calculated, which is the probability that the waves will exceed a threshold, let us say x_C in H_s. The hazard index is then defined as

$$H(x_C) = e^{-\left(\frac{x_C}{\lambda}\right)^k}. \qquad (6)$$

To compute the best-fit shape and scale parameters of the Weibull distribution for each of the eight control points, the maximum likelihood method (MLM) was used. This is the most widely used technique among parameter estimations and finds a value of the parameter that maximizes the likelihood function. The values of the Weibull parameters for each control point are presented in Table 6, which shows that the mean, standard deviation, and skewness computed from the model data are very similar to those estimated from the Weibull fit parameters. This thus highlights that the Weibull distribution well represents the behaviour of the H_s model data. The mean value and the corresponding variance of H_s at the Cesenatico station are larger than for the other control points, as the station is far from the coast with the highest water depth. The analysis results show that the fitted Weibull distributions have positive kurtosis, which indicates that the distribution has fat tails.

To evaluate the goodness of fit of the Weibull distribution, the classical chi-squared (χ^2) test was used. This test determines how well the theoretical distribution fits the given model data distribution. If the chi-squared value is lower than a critical χ^2 value, we retain the null hypothesis and conclude that there is no significant difference between the observed
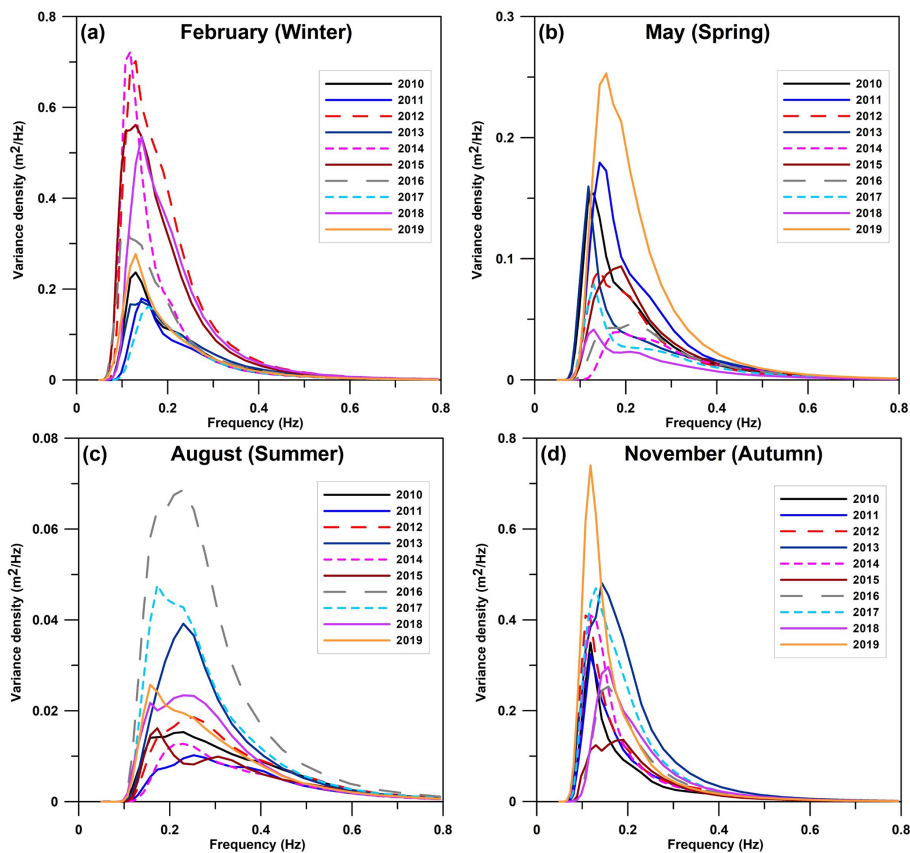
Figure 11. Simulated monthly mean wave spectra for the time slice 2010–2019 for **(a)** February (winter), **(b)** May (spring), **(c)** August (summer), and **(d)** November (autumn) at station 6 (Cesenatico; see Fig. 1c for location).

Table 6. The best-fit Weibull scale and shape parameters for H_s (columns 3–4) at the eight control points. Column 5 shows the estimated χ^2 values. Mean, variance, skewness, and kurtosis of H_s (columns 6–9) computed from the model data (left sub-columns) and from the Weibull fit parameters (right sub-columns) and the wave height hazard index (with threshold value X_c, $H_s = 1.08$ m) calculated with (Eq. 6) for the eight control points (indicated in the last column) along the Emilia-Romagna coastal strip.

Control points	Station name	Scale λ	Shape κ	χ^2	Mean (m) Model	Estim.	Variance (m^2) Model	Estim.	Skewness Model	Estim.	Kurtosis Model	Estim.	Hazard index
1	Lido di Pomposa	0.32	1.01	0.42	0.32	0.32	0.108	0.101	1.69	1.97	3.01	5.79	0.01
2	Porto Garibaldi	0.35	1.03	0.44	0.35	0.35	0.124	0.115	1.64	1.92	2.46	5.47	0.04
3	Casalborsetti	0.39	1.06	0.56	0.38	0.38	0.142	0.133	1.56	1.84	2.03	5.01	0.05
4	Lido Adriano	0.39	1.00	0.27	0.39	0.39	0.167	0.151	1.88	2.00	4.09	6.00	0.06
5	Foce Savio	0.35	1.00	0.48	0.35	0.35	0.133	0.125	1.68	2.00	2.67	6.02	0.05
6	Cesenatico	0.39	0.95	0.25	0.41	0.40	0.210	0.183	2.11	2.18	5.44	7.23	0.07
7	Rimini	0.36	0.96	0.35	0.37	0.37	0.169	0.147	2.16	2.13	5.91	6.88	0.06
8	Riccione	0.34	1.00	0.56	0.34	0.34	0.129	0.116	1.97	2.00	4.72	6.02	0.04

and the expected distributions. The estimated χ^2 values for each control points are given in Table 6. The decision rule for the χ^2 test depends on the level of significance (set to 0.05) and the degrees of freedom, defined as df $= N - $ np, where N is the number of bins (set to 30) and np is the number of distribution parameters (i.e. 2), so the critical value of χ^2 is 41.34 (taken from the χ^2 distribution table). Table 6 high-

lights that the two-parameter Weibull distribution fits the H_s data well.

In all the eight locations, since the shape value κ is close to 1, the fitted Weibull distributions behave like the exponential distribution. Figure 13 compares the Weibull distribution fit (red line) and the histogram of the model data for three relevant locations (Porto Garibaldi, Lido Adriano, and Ce-
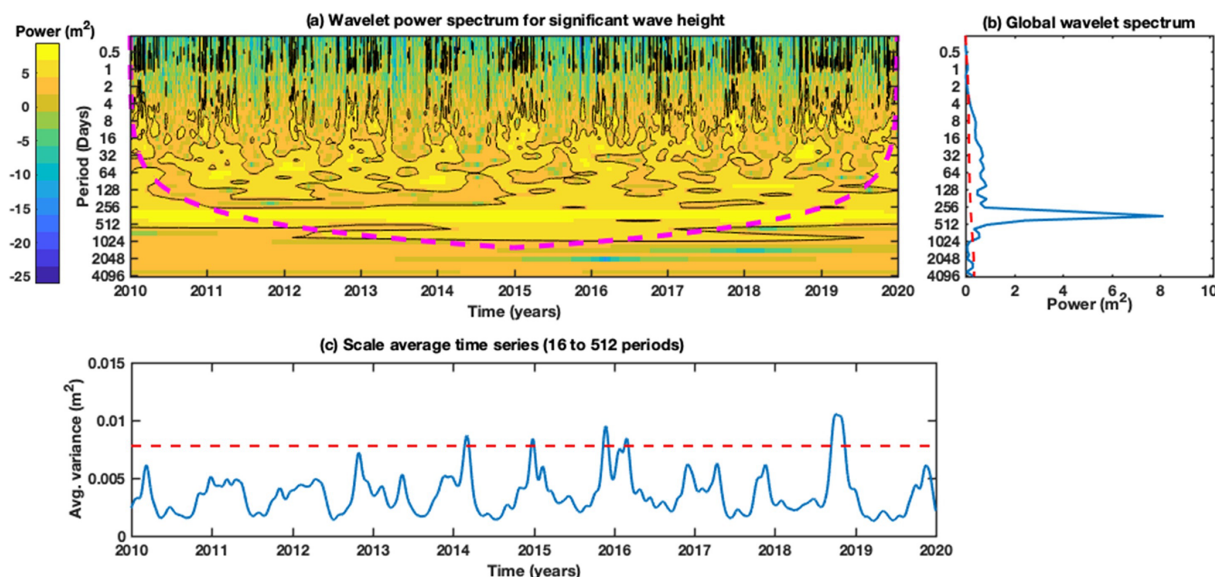
Figure 12. Wavelet analysis of wave climate time series (H_s in m) along the Emilia-Romagna coastal belt at station 6 (Cesenatico; see Fig. 1c for location) using mean model estimates. **(a)** Wavelet power spectrum for H_s. The colour bar stands for the formation of H_s variation. Power spectra intensity is represented by colours varying from navy blue colour (i.e. weak) to dark yellow (i.e. strong). The contours represent the total variance percentage, and the black contours indicate amplitude significance (greater than 95 % level). The dashed magenta line is the cone of influence (region of spectrum with the significant edge effects), where zero padding has reduced the variance. Figure 11a shows that power is concentrated in the 256–512 d band, which is a strong signal. **(b)** Global wavelet power spectrum, where the blue curve indicates the fast Fourier transform of the complete data. The dashed red line is the significance (95 %) for the global wavelet spectrum, assuming the same significance level and background spectrum as in wavelet power spectra. **(c)** Scaled averaged time series over a 16–512 d band showing variance of H_s. The dashed red line is the 95 % confidence level for H_s.

senatico). The two-parameter Weibull distribution appears to fit the data well in the coastal study area.

After evaluating the Weibull distribution fit and the statistical moments, we estimated the hazard index as shown in Table 6 (column 10) for a threshold value X_c (i.e. $H_s = 1.08$ m, 3 times the mean standard deviation). The hazards were shown to increase 7-fold from the northern control points (Lido di Pomposa) to Cesenatico and then to decrease again. In the future it will be interesting to compare the hazards for different coastal areas around the Adriatic Sea.

6   Summary and conclusions

To accurately simulate the wind-wave climate in the Emilia-Romagna coastal belt, a high-resolution numerical modelling study using unstructured-grid WW3 was executed for a 10-year period. The WW3 model was driven by the ECMWF analysis winds, and the model was validated with available wave buoy data at a coastal location. The sensitivity tests have shown the good accuracy of ST6+SHOWEX physics for wave hindcasts in the study area. The results of a comparison of model estimates with measurements were promising. An H_s correlation of 0.86 to 0.93 was found for the 10-year simulations with observed data. The underestimations in H_s were indicative of a negative bias (-0.076 to -0.016 m)

with an RMSE of 0.19 to 0.25 m. The comparison of T_m and T_p with buoy measurements revealed a correlation of 0.70 to 0.80 and 0.53 to 0.70 respectively, for the 10 years. Our database was then used to study and characterize the present climate of waves for the region, and a hazard index for extreme events was defined and computed. The following conclusions were drawn:

- The spatial mean wind speed for winter, spring, summer, and autumn varied in the range 1.1–2.9, 0.5–1.5, 0.5–1.8, and 0.5–2.4 m s^{-1} respectively. The lowest wind speeds were observed during spring and summer (1.5 and 1.8 m s^{-1}) considering the study domain, followed by autumn (2.4 m s^{-1}), and the highest wind speeds (2.9 m s^{-1}) were observed during winter seasons.

- The annual H_s mean in the ER domain varied from 0.08–0.6 m, and in the ER coastal belt the annual mean H_s was < 0.4 m owing to bathymetric features. In the ER coastal belt, the seasonal climatology of H_s in the winter showed a mean $H_s < 0.5$ m, while in spring and summer the H_s values were comparatively low ($H_s < 0.38$ and $H_s < 0.21$ m). The autumn H_s mean was < 0.4 m. It should be noted that there was more wave activity in winter and autumn than in spring and summer.
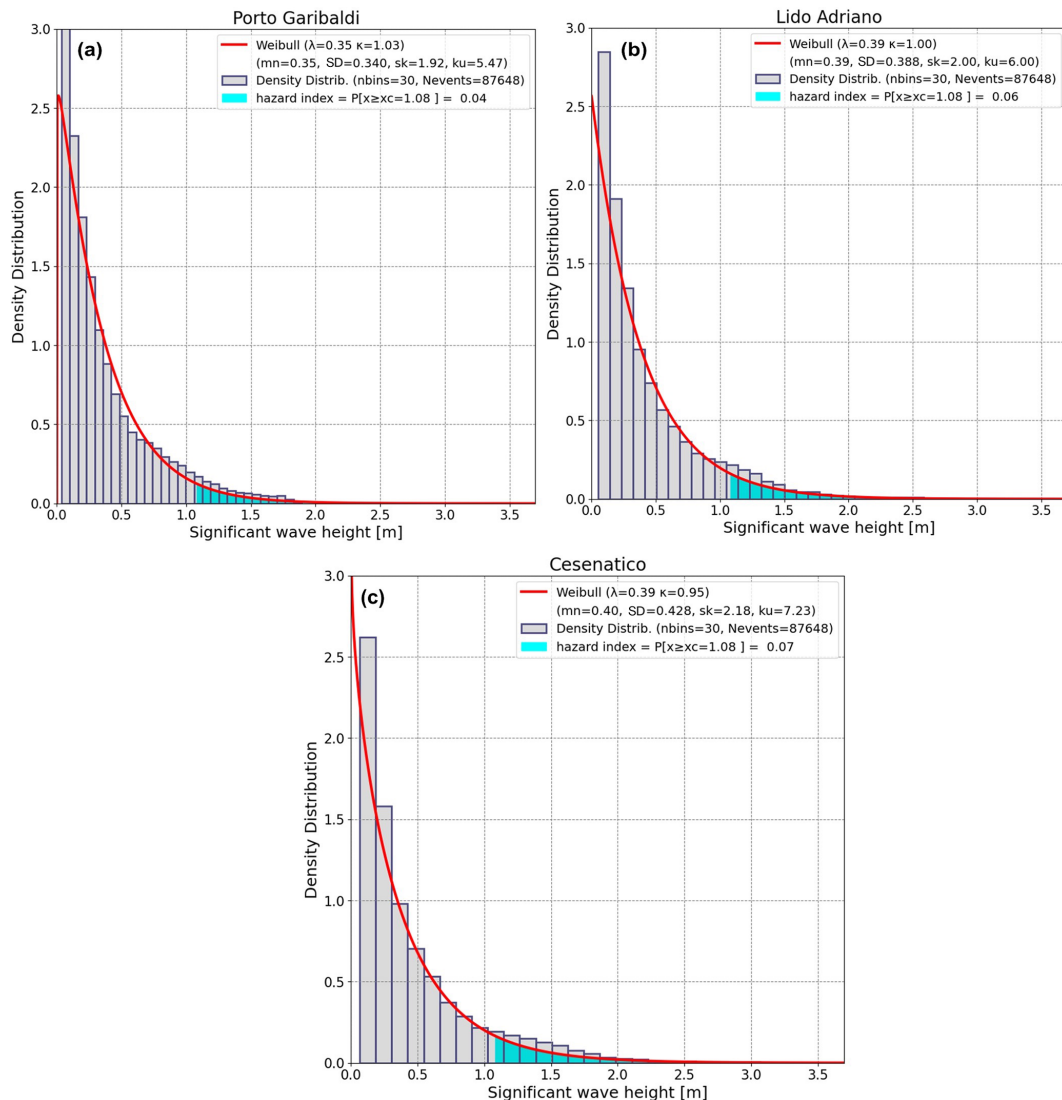
Figure 13. Comparison of the Weibull distribution fit (red line) to the histogram of the model data (2010–2019) for the control points: **(a)** Porto Garibaldi, **(b)** Lido Adriano, and **(c)** Cesenatico. The red line denotes the Weibull fit; the histograms represent the density distribution (seen in grey colour), and the hazard index is indicated in cyan colour (mn: mean; SD: standard deviation; sk: skewness; ku: kurtosis; nbins: number of bins; Nevents: number of events).

– The analysis of instantaneous spectra showed that during all seasons the spectra exhibited bi-modal characteristics (double-peaked), with a dominant occurrence percentage of 53 % in summer, while during spring, winter, and autumn the spectra also showed single-peaked spectra (31 %–33 %). The average spectra analysis showed peak frequencies of the order of 0.097 to 0.172 Hz, 0.107 to 0.229 Hz, 0.142 to 0.278 Hz, and 0.097 to 0.208 Hz for winter, spring, summer, and autumn seasons respectively.

– With the aid of a wavelet analysis tool, the power features (time–frequency) of H_s data showed substantial variability in H_s for a 10-year period, with the occur-

rence of monthly and seasonal periods. The 256–512 d band showed a higher power concentration which represents the seasonal frequency.

– The coastal control point time series was well fitted by a Weibull PDF. The Weibull at all control points was congruent with an exponential distribution. Using the Weibull PDF fit, we calculated a hazard index which indicated that for waves higher than 3 standard deviations from the mean, i.e. the highest hazard is reached at the Cesenatico station (hazard index of 0.07 (Fig. 13c) instead of 0.06 (Fig. 13b) and 0.04 (Fig. 13a)).

The limitation in the present study is the non-availability of wave spectra measurements at the coastal locations for val-

idation. Future study will aim to consider data assimilation (de Rosnay et al., 2022) and to have higher-resolution winds as forcings for the wave model. In the context of heavy-tailed data sets, the Weibull distribution may not represent the best description of the peak and tail. These limits can be overcome by adding more parameters such as the four-parameter exponentiated Weibull distribution (Mahmoudi et al., 2018) such that the extra shape parameter can provide more versatility regarding the distribution in the shape of the tails.

Another limitation is that a 10-year period would generally not be enough to bring out the complete climatological wave response to winds. ECMWF winds were too low resolution before 2010, and no downscaled limited-area meteorological forcing is available. Hence this 10-year period could be the first reference database for the prevailing wind-wave characteristics in the coastal belt for researchers and coastal engineers/designers. Future works should definitely deal with longer simulation periods and also higher-resolution winds.

Our analysis highlights the importance of long-term wave databases, which can aid in the design requirements of coastal engineering applications. It also demonstrates the useful application of PDFs to the estimate of hazards along coastal belts. The study also highlights the need for extensive wave spectra comparisons (Lobeto et al., 2021) with measurements for selected locations on the coastal belt, which will update the coastal wave database. The early detection of hazards such as coastal erosion and associated shoreline changes are still challenging (Le Cozannet et al., 2020) due to the non-availability of long-term observations. As reported by Vousdoukas et al. (2018), by the end of the century, the community encountering marine flooding is estimated to rise from 1.52 to 3.65 million, and considering global vulnerability (Luijendijk et al., 2018), low-lying nearshore regions (one-fourth) are retreating, and eroded land (Mentaschi et al., 2018) remains twice what is acquired. Better knowledge of the prevailing wave characteristics on the ER coastal belt will aid in predicting coastal impacts.

References

Aguirre, C., Rutllant, J. A., and Falvey, M.: Wind waves climatology of the Southeast Pacific Ocean, Int. J. Climatol., 37, 4288–4301, 2017.

Akpinar, A. and Komurcu, M. I.: Assessment of wave energy resource of the Black Sea based on 15-year numerical hindcast data, Appl. Energy, 101, 502–512, 2013.

Amarouche, K., Bingölbali, B., and Akpinar, A.: New wind-wave climate records in the Western Mediterranean Sea, Clim. Dynam., 58, 1899–1922, 2022.

Ardhuin, F., O'Reilly, W. C., Herbers, T. H. C., and Jessen, P. F.: Swell Transformation across the Continental Shelf. Part I: Attenuation and Directional Broadening, J. Phys. Oceanogr., 33, 1921–1939, 2003.

Ardhuin, F., Bertotti, L., Bidlot, J. R., Cavaleri, L., Filipetto, V., Lefevre, J. M., and Wittmann, P.: Comparison of wind and wave measurements and models in the western Mediterranean Sea, Ocean Eng., 34, 526–541, 2007.

Ardhuin, F., Rogers, W. E., Babanin, A. V., Filipot, J., Magne, R., Roland, A., van der Westhuysen, A., Queffeulou, P., Lefevre, J., Aouf, L., and Collard, F.: Semiempirical dissipation source functions for ocean waves. Part I: Definition, calibration, and validation, J. Phys. Oceanogr., 40, 1917–1941, 2010.

Arkhipkin, V. S., Gippius, F. N., Koltermann, K. P., and Surkova, G. V.: Wind waves in the Black Sea: results of a hindcast study, Nat. Hazards Earth Syst. Sci., 14, 2883–2897, https://doi.org/10.5194/nhess-14-2883-2014, 2014.

Armaroli, C. and Duo, E.: Validation of the coastal storm risk assessment framework along the emilia-romagna coast, Coast. Eng., 134, 159–167, 2018.

Armaroli, C., Ciavola, P., Masina, M., and Perini, L.: Run-up computation behind emerged breakwaters for marine storm risk assessment, J. Coast. Res., 56, 1612–1616, 2009.

Armaroli, C., Ciavola, P., Perini, L., Calabrese, L., Lorito, S., Valentini, A., and Masina, M.: Critical storm thresholds for significant morphological changes and damage along the Emilia-Romagna coastline, Italy, Geomorphology, 143–144, 34–51, 2012.

Armaroli, C., Duo, E., and Viavattene, C.: From Hazard to Consequences: Evaluation of Direct and Indirect Impacts of Flooding Along the Emilia-Romagna Coastline, Italy, Front. Earth Sci., 7, 203, https://doi.org/10.3389/feart.2019.00203, 2019.

Babanin, A. V.: Breaking and dissipation of ocean surface waves, Cambridge University Press, 480 pp., ISBN 9780511736162, https://doi.org/10.1017/CBO9780511736162., 2011.

Barbariol, F., Davison, S., Falcieri, F. M., Ferretti, R., Ricchi, A., Sclavo, M., and Benetazzo, A.: Wind Waves in the Mediterranean Sea: An ERA5 Reanalysis Wind-Based Climatology, Front. Mar. Sci., 8, 760614, https://doi.org/10.3389/fmars.2021.760614, 2021.

Battjes, J. A. and Janssen, J. P. F. M.: Energy loss and set-up due to breaking of random waves, in: 16th International Conference on Coastal Engineering, 27 August–3 September 1978, Hamburg, Germany, 569–587, https://doi.org/10.1061/9780872621909.034, 1978.

Benetazzo, A., Francesco, B., Paolo, P., Staneva, J., Behrens, A., Davison, S., Bergamasco, F., Sclavo, M., and Cavaleri, L.: Towards a unified framework for extreme sea waves from spectral models: rationale and applications, Ocean Eng., 219, 108263, https://doi.org/10.1016/j.oceaneng.2020.108263, 2021.

Bertotti, L., Canestrelli, P., Cavaleri, L., Pastore, F., and Zampato, L.: The Henetus wave forecast system in the Adriatic Sea, Nat. Hazards Earth Syst. Sci., 11, 2965–2979, https://doi.org/10.5194/nhess-11-2965-2011, 2011.

Bertotti, L., Cavaleri, L., Loffredo, L., and Torrisi, L.: Nettuno: Analysis of a Wind and Wave Forecast System for the Mediterranean Sea, Mon. Weather Rev., 141, 3130–3141, 2013.

Biolchi, L. G., Unguendoli, S., Bressan, L., and Valentini, A.: Recent developments in the forecasting chain at Arpae-Simc for the Emilia-Romagna (Northeast Italy) coastal areas, in: 9th Eu-

roGOOS International conference, Shom, Ifremer, EuroGOOS AISBL, May 2021, Brest, France, hal-03328370, 2021.

Biolchi, L. G., Unguendoli, S., Bressan, L., Giambastiani, B. M. S., and Valentini, A.: Ensemble technique application to an XBeach-based coastal Early Warning System for the Northwest Adriatic Sea (Emilia-Romagna region, Italy), Coast. Eng., 173, 104081, https://doi.org/10.1016/j.coastaleng.2022.104081, 2022.

Bonaldo, D., Bucchignani, E., Ricchi, A., and Carniel, S.: Wind storminess in the Adriatic Sea in a climate change scenario, Acta Adriat., 58, 195–208, 2017.

Bosserelle, C., Pattiaratchi, C., and Haigh, I.: Inter-annual variability and longer-term changes in the wave climate of western Australia between 1970 and 2009, Ocean Dynam., 62, 63–76, 2012.

Carter, D. J. T., Foale, S., and Webb, D. J.: Variations in global wave climate throughout the year, Int. J. Remote Sens., 12, 1687–1697, 1991.

Cavaleri, L.: The oceanographic tower Acqua Alta – activity and prediction of sea states at Venice, Coast. Eng., 39, 29–70, 2000.

Cavaleri, L. and Malanotte-Rizzoli, P.: Wind-wave prediction in shallow water: Theory and applications, J. Geophys. Res., 86, 10961–10973, 1981.

Cavaleri, L., Bertotti, L., and Lionello, P.: Extreme storms in the Adriatic Sea, In: Edge, B. L. Ed., in: Proceedings 22nd Int. Conf. on Coastal Eng., 2–6 July 1990, Delft, the Netherlands, 218–226, 3305, 1991.

Cavaleri, L., Abdalla, S., Benetazzo, A., Bertotti, L., Bidlot, J.-R., Breivik, Ø., Carniel, S., Jensen, R. E., Portilla-Yandun, J., Rogers, W. E., Roland, A., Sanchez-Arcilla, A., Smith, J. M., Staneva, J., Toledo, Y., van Vledder, G. P. and van der Westhuysen, A. J.: Wave modelling in coastal and inner seas, Prog. Oceanogr., 167, 164–233, 2018.

Cavaleri, L., Bajo, M., Barbariol, F., Bastianini, M., Benetazzo, A., Bertotti, L., Chiggiato, J., Davolio, S., Ferrarin, C., Magnusson, L., Papa, A., Pezzutto, P., Pomaro, A., and Umgiesser, G.: The October 29, 2018 storm in Northern Italy-An exceptional event and its modeling, Prog. Oceanogr., 178, 102178, https://doi.org/10.1016/j.pocean.2019.102178, 2019.

Cavaleri, L., Barbariol, F., Bastianini, M., Benetazzo, A., Bertotti, L., and Pomaro, A.: An exceptionally high wave at the CNR-ISMAR oceanographic tower in the Northern Adriatic Sea, Sci. Data, 8, 37, https://doi.org/10.1038/s41597-021-00825-x, 2021.

Ciavola, P., Harley, M. D., and den Heijer, C.: The RISC-KIT storm impact database: a new tool in support of DR, Coast. Eng., 134, 24–32, 2017.

Clementi, E., Oddo, P., Drudi, M., Pinardi, N., Korres, G., and Grandi, A.: Coupling hydrodynamic and wave models: first step and sensitivity experiments in the Mediterranean Sea, Ocean Dynam., 67, 1293–1312, 2017.

Cox, A. T. and Swail, V. R.: A global wave hindcast over the period 1958–1997: validation and climate assessment, J. Geophys. Res., 106, 2313–2329, 2001.

De Leo, F., De Leo, A., Besio, G., and Briganti, R.: Detection and quantification of trends in time series of significant wave heights: an application in the Mediterranean Sea, Ocean Eng., 202, 107155, https://doi.org/10.1016/j.oceaneng.2020.107155, 2020.

De Leo, F., Besio, G., and Mentaschi, L.: Trends and variability of ocean waves under RCP8.5 emission scenario in the Mediterranean Sea, Ocean Dynam., 71, 97–117, 2021.

de Rosnay, P., Browne, P., de Boisséson, E., Fairbairn, D., Hirahara, Y., Ochi, K., Schepers, D., Weston, P., Zuo, H., Alonso-Balmaseda, M., Balsamo, G., Bonavita, M., Borman, N., Brown, A., Chrust, M., Dahoui, M., De Chiara, G., English, S., Geer, A., Healy, S., Hersbach, H., Laloyaux, P., Magnusson, L., Massart, S., McNally, A., Pappenberger, F., and Rabier, F.: Coupled data assimilation at ECMWF: current status, challenges and future developments, Q. J. Roy. Meteorol Soc., 148, 2672–2702, https://doi.org/10.1002/qj.4330, 2022.

DHI group: MIKE 21 Spectral Wave Module, Scientific Documentation, Danish Hydraulic Institute (DHI), Holsholm, Denmark, p. 56, https://manuals.mikepoweredbydhi.help/2017/Coast_and_Sea/M21SW_Scientific_Doc.pdf (last access: 20 March 2022), 2017.

Dodet, G., Bertin, X., and Taborda, R.: Wave climate variability in the North-East Atlantic Ocean over the last six decades, Ocean Model., 31, 120–131, 2010.

Donatini, L., Lupieri, G., Contento, G., Feudale, L., Pedroncini, A., Cusati, L. A., and Crosta, A.: A high resolution wind and wave forecast model chain for the Mediterranean and Adriatic Sea, in: Vol. 1, Towards Green Marine Technology and Transport: Proceedings of the 16th International Conference of the International Maritime Association of the Mediterranean (IMAM2015), 21–24 September 2015, Pula, Croatia, edited by: Guedes Soares, C., Dejhalla, R., and Pavletic, D., University of Trieste, Trieste, Italy, CRC Press, 859–866, ISBN 9780429225604, https://doi.org/10.1201/b18855, 2015.

Donelan, M. A., Babanin, A. V., Young, I. R., and Banner, M. L.: Wave follower measurements of the wind-input spectral function. Part II. Parameterization of the wind input, J. Phys. Oceanogr., 36, 1672–1689, 2006.

Farda, A., Štěpánek, P., Halenka, T., Skalák, P., and Belda, M.: Model ALADIN in climate mode forced with ERA-40 reanalysis (coarse resolution experiment), Meteorol. J., 10, 123–130, 2007.

Fedor, N. G. and Stanislav, A. M.: Black Sea wind wave climate with a focus on coastal regions, Ocean Eng., 218, 108199, https://doi.org/10.1016/j.oceaneng.2020.108199, 2020.

Ferrarin, C., Valentini, A., Vodopivec, M., Klaric, D., Massaro, G., Bajo, M., De Pascalis, F., Fadini, A., Ghezzo, M., Menegon, S., Bressan, L., Unguendoli, S., Fettich, A., Jerman, J., Ličer, M., Fustar, L., Papa, A., and Carraro, E.: Integrated sea storm management strategy: the 29 October 2018 event in the Adriatic Sea, Nat. Hazards Earth Syst. Sci., 20, 73–93, https://doi.org/10.5194/nhess-20-73-2020, 2020.

Fiori, E., Zavatarelli, M., Pinardi, N., Mazziotti, C., and Ferrari, C. R.: Observed and simulated trophic index (TRIX) values for the Adriatic Sea basin, Nat. Hazards Earth Syst. Sci., 16, 2043–2054, https://doi.org/10.5194/nhess-16-2043-2016, 2016.

Gaeta, M. G., Samaras, A. G., Federico, I., Archetti, R., Maicu, F., and Lorenzetti, G.: A coupled wave–3-D hydrodynamics model of the Taranto Sea (Italy): a multiple-nesting approach, Nat. Hazards Earth Syst. Sci., 16, 2071–2083, https://doi.org/10.5194/nhess-16-2071-2016, 2016.

Gaeta, M. G., Bonaldo, D., Samaras, A. G., Carniel, S., and Archetti, R.: Coupled Wave-2D Hydrodynamics Modeling at the Reno River Mouth (Italy) under Climate Change Scenarios, Water, 10, 1380, https://doi.org/10.3390/w10101380, 2018.

Gorman, R. M., Bryan, K. R., and Laing, A. K.: Wave hindcast for the New Zealand region: deep-water wave climate, NZ J. Mar. Freshw. Res., 37, 589–612, 2003.

Harley, M. D., Valentini, A., Armaroli, C., Perini, L., Calabrese, L., and Ciavola, P.: Can an early-warning system help minimize the impacts of coastal storms? A case study of the 2012 Halloween storm, northern Italy, Nat. Hazards Earth Syst. Sci., 16, 209–222, https://doi.org/10.5194/nhess-16-209-2016, 2016.

Hasselmann, K., TBarnett, T. P., Bouws, E., Carlson, H., Cartwright, D. E., Enke, K., Ewing, J. A., Gienapp, H., Hasselmann, D. E., Kruseman, P., Meerburg, A., Muller, P., Olbers, D. J., Richter, K., Sell, W., and Walden, H.: Measurements of wind-wave growth and swell decay during the Joint North Sea Wave Project (JONSWAP), Ergänzungsheft zur Deutschen Hydrographischen Zeitschrift, Reihe A 12, 95 pp., http://resolver.tudelft.nl/uuid:f204e188-13b9-49d8-a6dc-4fb7c20562fc (last access: 20 March 2022), 1973.

Hemer, M. A., Church, J. A., and Hunter, J. R.: Variability and trends in the directional wave climate of the Southern Hemisphere, Int. J. Climatol., 30, 475–491, 2010.

Hemer, M. A., Wang, X. L., Weisse, R., and Swail, V. R.: Advancing wind-waves climate science, B. Am. Meteorol. Soc., 93, 791–796, 2012.

IDROSER: Progetto di Piano per la difesa del mare e la riqualificazione ambientale del litorale della Regione Emilia-Romagna, Regione Emilia-Romagna, Bologna, Italia, 365 pp., 1996.

IPCC: Climate Change 2007: The Physical Science Basis, in: Contribution of Working Group I to the Fourth Assessment Report of the Intergovernmental Panel on Climate Change, edited by: Solomon, S., Qin, D., Manning, M., Chen, Z., Marquis, M., Averyt, K. B., Tignor, M., and Miller, H. L., Cambridge University Press, Cambridge, UK, 996 pp., ISBN 978-0-521-88009-1, 2007.

IPCC: Climate Change 2021: The Physical Science Basis, in: Contribution of Working Group I to the Sixth Assessment Report of the Intergovernmental Panel on Climate Change, edited by: Masson-Delmotte, V., Zhai, P., Pirani, A., Connors, S. L., Péan, C., Berger, S., Caud, N., Chen, Y., Goldfarb, L., Gomis, M. I., Huang, M., Leitzell, K., Lonnoy, E., Matthews, J. B. R., Maycock, T. K., Waterfield, T., Yelekçi, O., Yu, R., and Zhou, B., Cambridge University Press, Cambridge, UK and New York, NY, USA, 2391 pp., https://doi.org/10.1017/9781009157896, 2021.

Kamranzad, B., Etemad-shahidi, A., and Chegini, V.: Assessment of wave energy variation in the Persian Gulf, Ocean Eng., 70, 72–80, 2013.

Katalinić, M., Ćorak, M., and Parunov, J.: Analysis of wave heights and wind speeds in the Adriatic Sea, in: Maritime Technology and Engineering Vol. 1, Proceedings of the MARTECH 2014, 2nd International Conference on Maritime Technology and Engineering, 15–17 October 2014, Lisabon, Portugal, edited by: Soares, C. G. and Santos, T. A., CRC Press/Balkema, Leiden, the Netherlands, 1389–1394, 2015.

Komen, G. J., Cavaleri, L., Donelan, M., Hasselmann, K., Hasselmann, S., and Janssen, P. A. E. M.: Dynamics and Modelling of Ocean Waves, Cambridge University Press, 532 pp., ISBN 9780511628955, https://doi.org/10.1017/CBO9780511628955, 1994.

Korres, G., Papadopoulos, A., Katsafados, P., Ballas, D., Perivoliotis, L., and Nittis, K.: A 2-year intercomparison of the WAM-

CYCLE4 and the WAVEWATCH-III wave models implemented within the Mediterranean Sea, Mediterr. Mar. Sci., 12, 129–152, 2011.

Korres, G., Ravdas, M., Zacharioudaki, A., Denaxa, D., and Sotiropoulou, M.: Mediterranean Sea Waves Analysis and Forecast (CMEMS MED-Waves, MedWAM3 system) (Version 1) set, CMEMS – Copernicus Monitoring Environment Marine Service, https://doi.org/10.25423/CMCC/MEDSEA_ANALYSISFORE, 2021.

Le Cozannet, G., Oliveros, C., Brivois, O., Giremus, A., Garcin, M., and Lavigne, F.: Detecting Changes in European Shoreline Evolution Trends Using Markov Chains and the Eurosion Database, Front. Mar. Sci., 7, 326, https://doi.org/10.3389/fmars.2020.00326, 2020.

Lionello, P.: The Climate of the Mediterranean Region, Elsevier, Amsterdam, https://doi.org/10.1016/C2011-0-06210-5, 2012.

Lionello, P. and Sanna, A.: Mediterranean wave climate variability and its links with NAO and Indian monsoon, Clim. Dynam., 25, 611–623, 2005.

Lionello P., Abrantes, F., Congedi, L., Dulac, F., Gacic, M., Gomis, D., Goodess, C., Hoff, H., Kutiel, H., Luterbacher, J., Planton, S., Reale, M., Schröder, K., Struglia, M. V., Toreti, A., Tsimplis, M., Ulbrich, U., and Xoplaki, E.: Introduction: Mediterranean Climate: Background Information in The Climate of the Mediterranean Region. From the Past to the Future, edited by: Lionello, P., Elsevier, Amsterdam, the Netherlands, XXXV–lXXX, ISBN 9780124160422, 2012.

Lobeto, H., Menendez, M., and Losada, I. J.: Projections of Directional Spectra Help to Unravel the Future Behavior of Wind Waves, Front. Mar. Sci., 8, 655490, https://doi.org/10.3389/fmars.2021.655490, 2021.

Luijendijk, A., Hagenaars, G., Ranasinghe, R., Fedor, B., Gennadii, D., and Stefan, A.: The State of the World's Beaches, Sci. Rep., 8, 6641, https://doi.org/10.1038/s41598-018-24630-6, 2018.

Mahmoudi, E., Meshkat, R. S., Kargar, B., and Kundu, D.: The Extended Exponentiated Weibull Distribution and its Applications, Statistica, 78, 363–396, 2018.

Mentaschi, L., Vousdoukas, M. I., Pekel, J.-F., Voukouvalas, E., and Feyen, L.: Global long-term observations of coastal erosion and accretion, Sci. Rep., 8, 12876, https://doi.org/10.1038/s41598-018-30904-w, 2018.

Morales-Márquez, V., Orfila, A., Simarro, G., and Marcos, M.: Extreme waves and climatic patterns of variability in the eastern North Atlantic and Mediterranean basins, Ocean Sci., 16, 1385–1398, https://doi.org/10.5194/os-16-1385-2020, 2020.

Muraleedharan, G., Unnikrishnan Nair, N., and Kurup, P. G.: Characteristics of long-term distributions of wave heights and periods in the eastern Arabian Sea, Indian J. Mar. Sci., 22, 21–27, 1993.

Muraleedharan, G., Kurup, P. G., and Unnikrishnan Nair, N.: Weibull model for shallow water wave height distribution and prediction, in: National Conference on Current Trends in Ocean Predictions with Special Reference to Indian Seas, Naval Physical and Oceanographic Laboratory, 22–23 December 1998, Kochi, Kerala, India, 80–85, 1998.

Muraleedharan, G., Unnikrishnan Nair, N., and Kurup, P. G.: Application of Weibull model for redefined significant wave height distributions, Proc. Indian Acad. Sci. Earth Planet. Sci., 108, 149–153, 1999.

Murphy, A. H.: What Is a Good Forecast? An Essay on the Nature of Goodness in Weather Forecasting, Weather Forecast., 8, 281–293, 1993.

Pandzic, K. and Likso, T.: Eastern Adriatic typical wind field patterns and large-scale atmospheric conditions, Int. J. Climatol., 25, 81–98, 2005.

Perini, L., Calabrese, L., Luciani, P., Olivieri, M., Galassi, G., and Spada, G.: Sea-level rise along the Emilia-Romagna coast (Northern Italy) in 2100: scenarios and impacts, Nat. Hazards Earth Syst. Sci., 17, 2271–2287, https://doi.org/10.5194/nhess-17-2271-2017, 2017.

Pranavam Ayyappan Pillai, U., Pinardi, N., Federico, I., Causio, S., Trotta, F., Unguendoli, S., and Valentini, A.: Data/codes used in the the Natural Hazards and Earth System Sciences (NHESS) publication titled "Wind-Wave Characteristics and extremes along the Emilia-Romagna coast" by Pranavam Ayyappan Pillai et al., 2022 (Version V1), Zenodo [code and data set], https://doi.org/10.5281/zenodo.6360348, 2022.

Qian, C., Jiang, H., Wang, X., and Chen, G.: Climatology of Wind-Seas and Swells in the China Seas from Wave Hindcast, J. Ocean Univ. China, 19, 90–100, https://doi.org/10.1007/s11802-020-3924-4, 2020.

Queffeulou, P. and Bentamy, A.: Analysis of Wave Height Variability Using Altimeter Measurements: Application to the Mediterranean Sea, J. Atmos. Ocean. Tech., 24, 2078–2092, 2007.

Ravdas, M., Zacharioudaki, A., and Korres, G.: Implementation and validation of a new operational wave forecasting system of the Mediterranean Monitoring and Forecasting Centre in the framework of the Copernicus Marine Environment Monitoring Service, Nat. Hazards Earth Syst. Sci., 18, 2675–2695, https://doi.org/10.5194/nhess-18-2675-2018, 2018.

Reistad, M., Breivik, Ø., Haakenstad, H., Aarnes, O. J., Furevik, B. R., and Bidlot, J. R.: A high-resolution hindcast of wind and waves for the North Sea, the Norwegian Sea, and the Barents Sea, J. Geophys. Res., 116, C05019, https://doi.org/10.1029/2010JC006402, 2011.

Rogers, W. E., Babanin, A. V., and Wang, D. W.: Observation-consistent input and whitecapping dissipation in a model for wind-generated surface waves: Description and simple calculations, J. Atmos. Ocean. Tech., 29, 1329–1346, 2012.

Romagnoli, C., Sistilli, F., Cantelli, L., Aguzzi, M., De Nigris, N., Morelli, M., Gaeta, M. G., and Archetti, R.: Beach Monitoring and Morphological Response in the Presence of Coastal Defense Strategies at Riccione (Italy), J. Mar. Sci. Eng., 9, 851, https://doi.org/10.3390/jmse9080851, 2021.

Russo, A., Coluccelli, A., Carniel, S., Benetazzo, A., Valentini, A., and Paccagnella, T.: Operational Models Hierarchy for Short Term Marine Predictions: The Adriatic Sea Example, in: IEEE MTS/IEEE OCEANS, Bergen, 1–6, https://doi.org/10.1109/OCEANS-Bergen.2013.6608139, 2013.

Sanuy, M., Duo, E., Jäger, W. S., Ciavola, P., and Jiménez, J. A.: Linking source with consequences of coastal storm impacts for climate change and risk reduction scenarios for Mediterranean sandy beaches, Nat. Hazards Earth Syst. Sci., 18, 1825–1847, https://doi.org/10.5194/nhess-18-1825-2018, 2018.

Sekovski, I., Armaroli, C., Calabrese, L., Mancini, F., Stecchi, F., and Perini, L.: Coupling scenarios of urban growth and flood hazards along the Emilia-Romagna coast (Italy), Nat. Hazards

Nat. Hazards Earth Syst. Sci., 22, 3413–3433, 2022

https://doi.org/10.5194/nhess-22-3413-2022

Earth Syst. Sci., 15, 2331–2346, https://doi.org/10.5194/nhess-15-2331-2015, 2015.

Semedo, A., Suselj, K., Rutgersson, A., and Sterl, A.: A global view on the wind sea and swell climate and variability from ERA-40, J. Climate, 24, 1461–1479, 2011.

Sepulveda, H. H., Queffeulou, P., and Ardhuin, F.: Assessment of SARAL/AltiKa wave height measurements relative to buoy, Jason-2, and Cryosat-2 data, Mar. Geod., 38, 449–465, 2015.

Sikiric, M. D., Damir, I., Roland, A., Ivatek-Shahdan, S., and Tudor, M.: Operational Wave Modelling in the Adriatic Sea with the Wind Wave Model, Pure Appl. Geophys., 175, 3801–3815, 2018.

Steppeler, J., G. Doms, U. Shatter, Bitzer, H. W., Gassmann, A., Damrath, U., and Gregoric, G.: Meso-gamma scale forecasts using the nonhydrostatic model LM, Meteorol. Atmos. Phys., 82, 75–96, 2003.

Sterl, A. and Caires, S.: Climatology, variability and extrema of ocean waves: The web-based KNMI/ERA-40 wave atlas, Int. J. Climatol., 25, 963–977, 2005.

Sterl, A., Komen, G. J., and Cotton, P. D.: Fifteen years of global wave hindcasts using winds from the European centre for medium-range weather forecasts reanalysis: validating the reanalyzed winds and assessing the wave climate, J. Geophys. Res., 103, 5477–5492, 1998.

Stopa, J. E. and Cheung, K. F.: Periodicity and patterns of ocean wind and wave climate, J. Geophys. Res.-Oceans, 119, 5563–5584, 2014.

Tolman, H. L.: A genetic optimization package for the Generalized Multiple DIA in WAVEWATCH III, Tech. Note 289, Ver. 1.0, NOAA/NWS/NCEP/MMAB, 21 pp., https://polar.ncep.noaa.gov/mmab/papers/tn289/MMAB_289_v1.0.pdf (last access: 20 March 2022), 2010.

Tolman, H. L.: A Generalized Multiple Discrete Interaction Approximation for resonant four-wave nonlinear interactions in wind wave models with arbitrary depth, Ocean Model., 70, 11–24, 2013.

Tolman, H. L.: A genetic optimization package for the Generalized Multiple DIA in WAVEWATCH III, Tech. Note 289, Ver. 1.4, NOAA/NWS/NCEP/MMAB, 21 pp. + Appendix, https://polar.ncep.noaa.gov/mmab/papers/tn289/MMAB_289_v1.4.pdf (last access: 20 March 2022), 2014.

Tolman, H. L., Balasubramaniyan, B., Burroughs, L. D., Chalikov, D. V., Chao, Y. Y., Chen, H. S., and Gerald, V. M.: Development and Implementation of Wind-Generated Ocean Surface Wave Models at NCEP, Weather Forecast., 17, 311–333, 2002.

Torrence, C. and Compo, G. P.: A practical guide to wavelet analysis, B. Am. Meteorol. Soc., 79, 61–78, 1998.

Umgiesser, G., Ferrari, C., Cucc, A., De Pascalis, F., Bellafiore, D., Ghezzo, M., and Bajo, M.: Comparative hydrodynamics of 10 Mediterranean lagoons by means of numerical modeling, J. Geophys. Res.-Oceans, 119, 2212–2226, 2014.

Umgiesser, G., Bajo, M., Ferrarin, C., Cucco, A., Lionello, P., Zanchettin, D., Papa, A., Tosoni, A., Ferla, M., Coraci, E., Morucci, S., Crosato, F., Bonometto, A., Valentini, A., Orlić, M., Haigh, I. D., Nielsen, J. W., Bertin, X., Fortunato, A. B., Pérez Gómez, B., Alvarez Fanjul, E., Paradis, D., Jourdan, D., Pasquet, A., Mourre, B., Tintoré, J., and Nicholls, R. J.: The prediction of floods in Venice: methods, models and uncertainty (review article), Nat. Hazards Earth Syst. Sci., 21, 2679–2704, https://doi.org/10.5194/nhess-21-2679-2021, 2021.

Valentini, A., Delli Passeri, L., Paccagnella, T., Patruno, P., Marsigli, C., Cesari, D., Deserti, M., Chiggiato, J., and Tibaldi, S.: The sea state forecast system of ARPA-SIM, Boll. Geofis. Teor. Appl., 48, 333–349, 2007.

Vousdoukas, M. I., Mentaschi, L., Voukouvalas, E., Bianchi, A., Dottori, F., and Feyen, L.: Climatic and socioeconomic controls of future coastal flood risk in Europe, Nat. Clim. Change, 8, 776–780, 2018.

Weibull, W.: A statistical distribution function of wide applicability, J. Appl. Mech., 18, 293–297, 1951.

Woolf, D. K., Challenor, P. G., and Cotton, P. D.: Variability and predictability of the North Atlantic wave climate, J. Geophys. Res., 107, 3145–3158, 2002.

WW3DG – WW3 Development Group: User manual and system documentation of WW3 v.5.16, NOAA, http://polar.ncep.noaa.gov/waves/wavewatch/manual.v5.16.pdf (last access: 20 March 2022), 2016.

Yamaguchi, M.: Approximate expressions for integral properties of the JONSWAP spectrum, Proc. Jpn. Soc. Civ. Eng., 345, 149–152, 1984.

Young, I. R.: Seasonal variability of the global ocean wind and wave climate, Int. J. Climatol., 19, 931–950, 1999.

Young, I. R. and Donelan, M. A.: On the determination of global ocean wind and wave climate from satellite observations, Remote Sens. Environ., 215, 228–241, 2018.

Young, I. R. and Holland, G. J.: Atlas of the Oceans: Wind and Wave Climate, Pergamon Press, 241 pp., ISBN 13:978-0080425191, 1996.

Young, I. R., Zieger, S., and Babanin, A. V.: Global trends in wind speed and wave height, Science, 332, 451–455, 2011.

Young, I. R., Fontaine, E., Liu, Q., and Babanin, A. V.: The wave climate of the Southern Ocean, J. Phys. Oceanogr., 50, 1417–1433, 2020.

Zheng, C. W. and Li, C. Y.: Variation of the wave energy and significant wave height in the China Sea and adjacent waters, Renew. Sustain. Energ. Rev., 43, 381–387, 2015.

Zheng, K., Sun, J., Guan, C., and Shao, W.: Analysis of the global swell and wind sea energy distribution using WAVEWATCH III, Adv. Meteorol., 2016, 1–9, https://doi.org/10.1155/2016/8419580, 2016.

Zieger, S., Babanin, A. V., Rogers, W. E., and Young, I. R.: Observation-based source terms in the third-generation wave model WAVEWATCH, Ocean Model., 96, 2–25, 2015.

https://doi.org/10.5194/nhess-22-3413-2022

Nat. Hazards Earth Syst. Sci., 22, 3413–3433, 2022